Science in China: *Series B Chemistry* 2006 Vol.49 No.1 21—43

DOI: 10.1007/s11426-005-0190-7

Applications of self-consistent field theory in polymer systems*

YANG Yuliang, QIU Feng, TANG Ping & ZHANG Hongdong

The Key Laboratory of Molecular Engineering of Polymers of Ministry of Education of China, Department of Macromolecular Science, Fudan University, Shanghai 200433, China
Correspondence should be addressed to Yang Yuliang (email: ylyang@fudan.ac.cn)

Received August 30, 2005; accepted August 31, 2005

Abstract The self-consistent field theory (SCFT) based upon coarse-grained model is especially suitable for investigating thermodynamic equilibrium morphology and the phase diagram of inhomogeneous polymer systems subjected to phase separation. The advantage of this model is that the details of the chain such as the architecture of the chain and the sequence of blocks can be considered. We present here an overview of SCFT approach and its applications in polymeric systems. In particular, we wish to focus on our group's achievements in applications of SCFT in such fields: simulation of microphase separation morphologies of multiblock copolymers with a complex molecular architecture, interactions between brush-coated sheets in a polymer matrix, mixtures of flexible polymers and small molecular liquid crystals at the interface, shapes of polymer-chain-anchored fluid vesicles, self-assembled morphologies of block copolymers in dilute solution, and so on. Finally, the further developments as well as the perspective applications of SCFT are discussed.

Keywords: self-consistent field theory, block copolymer, microphase separation.

1 Introduction

Owing to the specificity of the long chain, polymers present complexity and versatility. These molecules in the system can be various in their topological structures, such as linear, star, comb or circle structures; meanwhile they can be polymerized by different methods or in different types of monomers to make the diblock, triblock or random copolymers. Due to the great internal free degree, the repulsive interaction between the chemically different blocks and chemical connectivity of chains drives the system to self-assemble into a variety of ordered structures[1]. Obviously, the biggest challenge is to deal with phase behavior and morphologies of block copolymers with such a complicate molecular architecture.

During the last four decades, weak-segregated and strong-segregated polymer theories have been developed based on statistical mechanics[2−6]. So far, one of the most wildly used theories is the SCFT[6], which is the most accurate with only least hypothesis on the level of mean-field and can be applied to describing the configuration of polymer chains in detail. In particular, thermodynamic equilibrium properties of block copolymer systems have been treated successfully by

* This review was recommended by Prof. Li Lemin, member of editorial board of *Science in China*.

SCFT, which can consider not only topological structures of chains (linear, star, comb, etc.) but also other details such as how the chain length and the interaction between segments influence the phase behavior. Furthermore, SCFT is a precise theory of wide application ranging from weak-segregated to strong-segregated conditions.

In this article, we will discuss the thermodynamic equilibrium and meta-stable properties of polymeric systems by using SCFT, especially combining our recent new progresses. We focus on the fields of the equilibrium phase structures, such as the meso-scale phases of block copolymers, the equilibrium state of liquid-crystal containing systems, the interaction between nano-particals and branched polymer chains, and shapes of polymer chains anchored vesicles, etc.

2 SCFT framework

2.1 Path integral of chains

The essential part of SCFT is the so-called coarse-graining method, in which a chain of the length N is simplified as a Brown particle's random walking path after N steps diffusion, keeping the profile of long chain characteristics and neglecting the details on atoms and groups, as shown in Fig. 1.

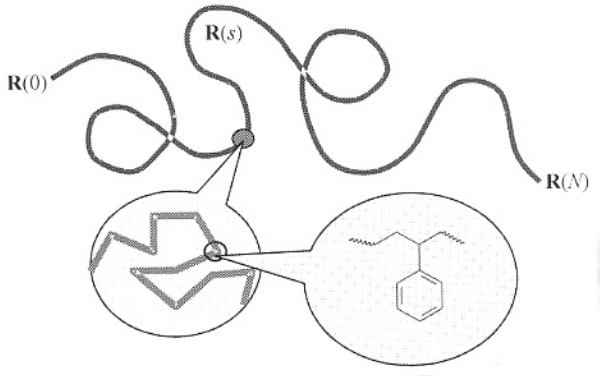

Fig. 1. Schematics of coarse-graining course. If we neglect the details on atoms and groups, the whole chain can be regarded as an array of coarse-grained segments. Furthermore, the chain can be simplified as a smooth curve (path) $\mathbf{R}(s)$, $0<s<N$.

If we regard the path variable s as time and define $\mathbf{R}(s)$ to be the position vector function, the Hamiltonian of the Brown particle in a time depending external field $V(\mathbf{R}(s))$ is given by[7]:

$$H_{\text{total}} = \frac{3}{2b^2}\int_0^N \mathrm{d}s\left[\frac{\mathrm{d}\mathbf{R}(s)}{\mathrm{d}s}\right]^2 + \frac{1}{kT}\int_0^N \mathrm{d}sV[\mathbf{R}(s)] = H^0 + H_{\text{int}}, \quad (1)$$

where the first term is the kinetic energy of the Brown particle, while the second is the potential energy, and b is the Kuhn length. We define $Q(\mathbf{r}, \mathbf{r}'; s)$ to be the probability of a particle starting its travel from position $\mathbf{r}'$ and stopping at $\mathbf{r}$ in the time interval $(0, s)$. Sum over all spatial curves of length N between $\mathbf{r}'$ and $\mathbf{r}$, then the partition function can be obtained in terms of the Feynman formulas used for quantum dynamics[7]:

$$Q(\mathbf{r},\mathbf{r}';s) = A\int_{\mathbf{R}(0)=\mathbf{r}'}^{\mathbf{R}(N)=\mathbf{r}} D\mathbf{R}(s)\exp\left[-\frac{3}{2b^2}\int_0^N \mathrm{d}s\left[\frac{\partial\mathbf{R}(s)}{\partial s}\right]^2 - \frac{1}{kT}\int_0^N \mathrm{d}sV[\mathbf{R}(s)]\right]. \quad (2)$$

Here, the $\int D\mathbf{R}_\alpha(s)$ denotes functional integrations over all possible conformations, called the path integration. Obviously, $Q(\mathbf{r}, \mathbf{r}'; s)$ should satisfy the diffusion equation[7]:

$$\left(\frac{\partial}{\partial s} - \frac{b^2}{6}\nabla^2 + \frac{1}{kT}V(\mathbf{r})\right)Q(\mathbf{r},\mathbf{r}';s) = \delta(\mathbf{r}-\mathbf{r}')\delta(s), \quad (3)$$

subject to the initial condition $Q(\mathbf{r}, \mathbf{r}'; 0) = \delta(\mathbf{r}-\mathbf{r}')$. Actually, this is Schrödinger function with the imaginary time. With the aids of well-developed methods in quantum physics, the partition function of a single chain may be solved.

The revolution thought as described above was first introduced by the British theoretical physicist Edwards in 1965 when he was working on the size of a self-avoid walking coil[8,9]. Actually, this problem had been solved by Flory in the nineteen fifties by simply estimating the polymer's configuration entropy and repulsion energy, obtaining a scaling exponent of 3/5[10]. But Edwards did not know Flory's work at that time. He proved that the spatial figure of a self-avoid walking chain can be explained as the path of a particle diffusing in an external field $V(\mathbf{r})$, and the movement function has the same form of Schrödinger function with imaginary time. Edwards followed this idea and obtained a self-avoid walking chain's gyration radius $R_G \propto N^{3/5}$, in good agreement with Flory's previous

results. The profound meaning in Edwards' work is that it was the first time to compare the configuration of a polymer chain with the movement of a particle. It revealed the deep relationship between polymer physics and the quantum field theory. The assistance from quantum field theory[11] has greatly accelerated the development of polymer condensed physics.

2.2 Mean filed theory of many-chain systems

As a starting point in the derivation of the theory, the partition function of the system is required. Considering a mixture of α components with the number of the αth component being n_α, the partition function of the system in the canonical ensemble is given by

$$Z=\left(\prod_\alpha \frac{1}{\Lambda_\alpha^{3n_\alpha} n_\alpha !}\right)\int\left[\prod_\alpha D^{n_\alpha}\mathbf{R}_\alpha(s)\right]\mathrm{e}^{-H_{\text{total}}[\{\mathbf{R}_\alpha(s)\}]}, \tag{4}$$

where Λ_α is the thermal deBrogie wavelength of the α component. The total Hamilton of this system can be written as

$$H_{\text{total}}[\{\mathbf{R}_\alpha(s)\}]=\sum_\alpha n_\alpha H_\alpha^0[\mathbf{R}_\alpha(s)]+H_{\text{int}}[\{\mathbf{R}_\alpha(s)\}]. \tag{5}$$

In the similar way, the grand canonical partition function of this system can be expressed in the following form:

$$\Xi=\sum_{\{n_\alpha\}}\left(\prod_\alpha \frac{\mathrm{e}^{\beta\mu_\alpha n_\alpha}}{\Lambda_\alpha^{3n_\alpha} n_\alpha !}\right)\int\left[\prod_\alpha D^{n_\alpha}\mathbf{R}_\alpha(s)\right]\mathrm{e}^{-H_{\text{total}}[\{\mathbf{R}_\alpha(s)\}]}, \tag{6}$$

where μ_α is the chemical potential of the α component.

The above-described partition function can be used in a wide range of applications. We consider a polymeric system which consists of n_α polymer chains. Each chain consists of N_α monomers of species κ. The polymer can then be represented by continuous-space curves $\mathbf{R}_\alpha(s)$, with s varying between 0 and N_α. The distribution of monomers κ on the chains is conveniently described by function $\gamma_\alpha^\kappa(s)=\delta[\text{type}_\alpha(s)-\kappa]$, which meets $\sum_\kappa \gamma_\alpha^\kappa(s)=1$, where $\text{type}_\alpha(s)$ is defined as the type of the sth monomer on the kind of α chain. For a given configuration $\{\mathbf{R}_\alpha(s)\}$, one can define a local monomer density operator $\hat{\rho}_\kappa(\mathbf{r})$ [12]:

$$\hat{\rho}_\kappa(\mathbf{r})=\sum_\alpha\sum_{i=0}^{n_\alpha}\int_0^{N_\alpha}\mathrm{d}s\,\delta[\mathbf{r}-\mathbf{R}_\alpha^i(s)]\gamma_\alpha^\kappa(s). \tag{7}$$

Further considering the orientation of polymer segment in some systems such as liquid crystals, another oriented order parameter is needed[13]:

$$\hat{S}^{ij}(\mathbf{r})=\sum_\kappa\sum_\alpha\sum_{i=0}^{n_\alpha}\int_0^{N_\alpha}\mathrm{d}\tau\,\delta[\mathbf{r}-\mathbf{R}_\alpha^i(s)]\gamma_\alpha^\kappa(s)\cdot\left[u_\alpha^{i,i}(s)u_\alpha^{i,j}(s)-\frac{1}{3}\delta^{ij}\right], \tag{8}$$

where $u_\alpha^i(s)$ is the orientation of the s segment on the i molecule of α component. In the system of polyelectrolyte, there are relevant definitions of the density operator[14]. Thus, the interaction Hamiltonian can be written as

$$H_{\text{int}}[\{\mathbf{R}_\alpha(s)\}]=H_{\text{int}}[\{\hat{\rho}_\kappa(\mathbf{r})\}], \tag{9}$$

where $\hat{\rho}_\kappa(\mathbf{r})$ denotes all kinds of density operators which depend on H_{int}.

Here, it is useful to introduce the collective variables of density operators, $\hat{\rho}_\kappa=\langle\hat{\rho}_\kappa\rangle\equiv\rho_\kappa$ to solve the partition function readily. It is useful to introduce δ-functions and their Fourier transforms:

$$\begin{aligned}&\int D\rho_\kappa\delta[\rho_\kappa-\hat{\rho}_\kappa]=1,\\ &\delta[\rho_\kappa-\hat{\rho}_\kappa]=\int DW_\kappa\mathrm{e}^{-iW_\kappa(\rho_\kappa-\hat{\rho}_\kappa)},\end{aligned} \tag{10}$$

where W_κ is conjugate potential of density field ρ_κ. This is called Hubbard-Stratonovich transformation and also called Edwards transformation in the theory of polymeric statistics[15]. Then, the partition function is transformed into:

$$Z=\int\left[\prod_\kappa(D\rho_\kappa DW_\kappa)\right]\mathrm{e}^{-\beta F[\{\rho_\kappa(\mathbf{r}),W_\kappa(\mathbf{r})\}]}, \tag{11}$$

where the functional is $\beta F = F/kT$:

$$\beta F=H_{\text{int}}-\int\mathrm{d}\mathbf{r}\sum_\kappa W_\kappa\rho_\kappa-\sum_\alpha n_\alpha\ln\frac{Q_\alpha[\{W_\kappa\}]}{n_\alpha}, \tag{12}$$

where Q_α denotes the partition function of the α component in the potential field W_κ.

$$\begin{aligned}Q_\alpha[\{W_\kappa\}]&=\int D\mathbf{R}_\alpha(s)\mathrm{e}^{-H_\alpha^0[\mathbf{R}_\alpha(s)]}\mathrm{e}^{-\int_0^{N_\alpha}\mathrm{d}s\sum_\kappa W_\kappa[\mathbf{R}_\alpha(s)]\gamma_\alpha^\kappa(s)}\\&=\int\mathrm{d}\mathbf{r}q_\alpha(\mathbf{r},N_\alpha),\end{aligned} \tag{13}$$

where $q_\alpha(\mathbf{r}, N_\alpha)$ is the end segment distribution function and is defined as

$$q_\alpha(\mathbf{r},s)=\int D\mathbf{R}_\alpha(s)\mathrm{e}^{-H_\alpha^0[\mathbf{R}_\alpha(s)]}\mathrm{e}^{-\sum_\kappa\int_0^s \mathrm{d}s' W_\kappa[\mathbf{R}_\alpha(s')]} \cdot\delta\left[\mathbf{R}_\alpha(s)-\mathbf{r}\right], \tag{14}$$

where $q_\alpha(\mathbf{r}, s)$ represents the probability distribution of monomer s at $\mathbf{r}$.

For the components which have no internal configuration, such as solvent, rigid-rod, rigid sphere etc., the Hamilton of these components is taken to be H_α^0= 0, and thereby the distribution function of chain segment is

$$q_\alpha(\mathbf{r})=\mathrm{e}^{-\int_0^{N_\alpha}\mathrm{d}s\sum_\kappa W_\kappa(\mathbf{r})\gamma_\alpha^\kappa(s)}. \tag{15}$$

For flexible polymers, the entropy due to the internal conformations should be included. The entropy can be obtained from the "string" with Kuhn length of b, and thus the combination of corresponding Hamiltonian and the interaction Hamiltonian is given by

$$\begin{aligned} H_\alpha^0&=\int_0^{N_\alpha}\mathrm{d}s\sum_\kappa\gamma_\alpha^\kappa(s)\frac{3}{2b_\kappa^2}\left[\frac{\mathrm{d}\mathbf{R}_\alpha(s)}{\mathrm{d}s}\right]^2,\\ H_{\mathrm{int}}&=\frac{1}{2}\int_0^{N_\alpha}\int_0^{N_{\alpha'}}\mathrm{d}s\mathrm{d}s'\sum_\kappa\gamma_\alpha^\kappa(s)\sum_{\kappa'}\gamma_{\alpha'}^{\kappa'}(s')\varepsilon_{\kappa\kappa'}\\ &\quad\cdot\delta[\mathbf{R}_\alpha(s)-\mathbf{R}_{\alpha'}(s')], \end{aligned} \tag{16}$$

where $3/2b_\kappa^2$ is the spring constant. Such as the block polymer, the two ends of chains are distinct and a second end-segment distribution function $q_\alpha^*(\mathbf{r}, s)$ is needed. $q_\alpha(\mathbf{r}, s)$ and $q_\alpha^*(\mathbf{r}, s)$ satisfy the following modified diffusion equation[7], respectively:

$$\begin{aligned} \frac{\partial q_\alpha(\mathbf{r},s)}{\partial s}&=\sum_\kappa\gamma_\alpha^\kappa(s)\left[\frac{b_\kappa^2}{6}\nabla^2-W_\kappa(\mathbf{r})\right]q_\alpha(\mathbf{r},s),\\ \frac{\partial q_\alpha^*(\mathbf{r},s)}{\partial s}&=-\sum_\kappa\gamma_\alpha^\kappa(s)\left[\frac{b_\kappa^2}{6}\nabla^2-W_\kappa(\mathbf{r})\right]q_\alpha^*(\mathbf{r},s), \end{aligned} \tag{17}$$

with initial condition $q_\alpha(\mathbf{r}, 0)$=1 and $q_\alpha^*(\mathbf{r}, N_\alpha)=1$, respectively.

For semi-flexible polymers, the configuration is affected by the bending rigidity as well. Rather than the Gaussian chain model, the worm-like chain model is adopted. The detailed expression of the Hamiltonian for semi-flexible chains can be found in ref. [16].

After Hubbard-Stratonovich transformation, the grand canonical partition function and the grand canonical potential can be written as

$$\begin{aligned} \Xi&=\int\left[\prod_\kappa(D\rho_\kappa DW_\kappa)\right]\mathrm{e}^{-\beta G[\{\rho_\kappa(\mathbf{r}),W_\kappa(\mathbf{r})\}]},\\ \beta G&=H_{\mathrm{int}}-\int\mathrm{d}\mathbf{r}\sum_\kappa W_\kappa\rho_\kappa+\sum_\alpha\frac{\mathrm{e}^{\beta\mu}Q_\alpha[\{W_\kappa\}]}{\Lambda_\alpha}, \end{aligned} \tag{18}$$

where $\sum_{n_\alpha=0}^{\infty}\frac{A^{n_\alpha}}{n_\alpha!}=\mathrm{e}^A$.

Assume that there are only short-range interactions in the system of flexible polymer, and thus the Flory-Huggins interaction parameter is taken to be $\chi_{\kappa\kappa'}=\frac{1}{2}(\varepsilon_{\kappa\kappa}+\varepsilon_{\kappa'\kappa'})-\varepsilon_{\kappa\kappa'}$ and the interaction Hamiltonian reads:

$$H_{\mathrm{int}}=\frac{1}{2}\sum_{\kappa,\kappa'}\chi_{\kappa\kappa'}\int\mathrm{d}\mathbf{r}\rho_\kappa(\mathbf{r})\rho_{\kappa'}(\mathbf{r}). \tag{19}$$

For liquid crystals, the interaction Hamiltonian is[13]

$$H_{\mathrm{int}}=\nu\int\mathrm{d}\mathbf{r}S^{ij}(\mathbf{r}):S^{ij}(\mathbf{r}), \tag{20}$$

where ν is Maier-Saupe interaction parameter, denoting anisotropy interactions due to the orientation.

2.3 Mean-field approximation (saddle-point approximation)

Although the free energy functional βF and βG can be obtained according to eqs. (12) and (18), the exact evaluation of the integral of functional is not possible. In the self-consistent mean-field theory, many interacting chains are reduced to that of independent chains subject to an external (mean) field, created by the other chains. Owing to the mean-field approximation, the functional can be evaluated by using a saddle-point technique. Differentiating eq. (12), we can obtain the minimum of the integrand. In this case, $F\approx F^{\mathrm{MF}}=F^{\mathrm{SCFT}}=F(\phi_\kappa, \omega_\kappa)=-k_{\mathrm{B}}T\ln Z$, where ϕ_κ and ω_κ are saddle point values under the condition of the minimum free energy. The SCFT equations are as follows:

$$\omega_\kappa=\frac{\delta H_{\mathrm{int}}}{\delta\rho_\kappa}, \tag{21}$$

$$\phi_\kappa(\mathbf{r})=-\sum_\alpha\frac{n_\alpha}{Q_\alpha}\frac{\delta Q_\alpha}{\delta W_\kappa}, \tag{22}$$

where

$$\frac{\delta Q_\alpha}{\delta W_\kappa}=\int D\mathbf{R}_\alpha(s)\mathrm{e}^{-H_\alpha^0[\mathbf{R}_\alpha(s)]}\mathrm{e}^{\int_0^{N_\alpha}\mathrm{d}s\sum_\kappa\omega_\kappa|\mathbf{R}_\alpha(s)|\gamma_\alpha^\kappa(s)}$$

$$\cdot \int_0^{N_\alpha} \mathrm{d}\tau \gamma_\alpha^\kappa(s)\delta[\mathbf{r}-\mathbf{R}_\alpha(s)]$$

$$= \int_0^{N_\alpha} \mathrm{d}s \gamma_\alpha^\kappa(s) \int D\mathbf{R}_\alpha(s) \Big\{ \mathrm{e}^{-H_\alpha^0[\mathbf{R}_\alpha(s)]}$$

$$\cdot \mathrm{e}^{\int_\tau^{N_\alpha} \mathrm{d}s' \sum_\kappa \omega_\kappa |\mathbf{R}_\alpha(s')| \gamma_\alpha^\kappa(s')}$$

$$\cdot \mathrm{e}^{\int_0^\tau \mathrm{d}s' \sum_\kappa \omega_\kappa |\mathbf{R}_\alpha(s')| \gamma_\alpha^\kappa(s') \delta[\mathbf{r}-\mathbf{R}_\alpha(s)]} \Big\}$$

$$= \int_0^{N_\alpha} \mathrm{d}s \gamma_\alpha^\kappa(s) q_\alpha(\mathbf{r},s) q_\alpha^*(\mathbf{r},s), \quad (23)$$

where $q_\alpha(\mathbf{r},\tau)$ and $q_\alpha^*(\mathbf{r},\tau)$ are end-segment distribution functions, respectively, satisfying diffusion equation (17). For clarity, the old density and potential ρ_κ and W_κ are replaced with saddle point values ϕ_κ and ω_κ. ω_κ is often called self-consistent molecular potential.

In general, the system is often subjected to different confinements. The most common is the impressibility, namely $\sum_\kappa \rho_\kappa = \rho_0$. In terms of a Lagrange multiplier, the confinement is introduced to the free energy directly, for example, $\int \mathrm{d}\mathbf{r}\xi(\mathbf{r})\left[\sum_\kappa \rho_\kappa(\mathbf{r}) - \rho_0\right]$. $\xi(\mathbf{r})$ is introduced to ensure the impressibility condition of the system and is given by

$$\omega_\kappa = \frac{\delta H_{\mathrm{int}}}{\delta \rho_\kappa} + \xi(\mathbf{r}). \quad (24)$$

ω and ϕ are solved by self-consistently iterative procedure, and then the partition function of a single chain and further the free energy of the system are obtained. Moreover, the stability of different structures can be verified by checking the free energy.

We must note that the above described mean field approximation does not consider the concentration fluctuation, which is asymptotically exact when the molecular weight is high enough and the system is far beyond the critical phase transition temperature. We also note that the distribution function $q_\alpha(\mathbf{r},\tau)$ and $q_\alpha^*(\mathbf{r},\tau)$ are not only used to calculate the concentrations of different species, but also keep the information about the conformation of the chain, which can be used to obtain the properties of the chains at the interface or confined to the wall.

The numerical implementation of the above self-consistent equations (21)—(24) with diffusion equation (17) first proposed by Matsen and Schick[6] has been successfully used to calculate the phase behavior of diblock copolymers. However, this method requires *prior* assumed mesophase symmetry and thus the discovery of new complex morphologies is limited. In recent years, real space implementation SCFT directly using a combinatorial screening algorithm proposed by Drolet and Fredrickson[17] has been extensively used to explore the phase structure of complex multiblock copolymers. The algorithm consists of randomly generating the initial values of the fields $\omega_\kappa(\mathbf{r})$. Eqs. (21)—(24) are solved iteratively until the solution becomes self-consistent. We refer the interested reader to see refs. [12, 17] for details.

3 Applications of SCFT in polymeric systems

3.1 Microphase morphologies of complex block copolymers

A block copolymer is a chain molecular consisting of two or more chemically different homopolymers joined covalently. In general, due to the intricate balance of the interfacial energy and conformation entropy, the block copolymers microphase separate to form a rich variety of periodic nanostructures. Block copolymers are useful in many applications, such as thermoplastic elastomers, rubber toughened plastics, adhesives, coating, and so on[18]. These nanostructures are thermodynamically stable and a typical periodicity is in the range 5—100 nm, and thus can be used for a kind of nanocomosites. In recent ten years, self-assembled morphologies of block copolymers may be used to template the fabrication of nanostructures in other materials, such as nanodots or nanotube array[19], mesoporous solids[20] and photon crystals[21]. The prediction of microphase separation morphologies of AB diblock copolymers has been studied successfully for many years due to the exciting development of condensed physics theory in recent two decades. Our group investigated the self-assembled morphologies and phase diagram of ABC triblocks with different architectures[22,23].

For block copolymers, there exist polymerized block numbers and topological structures. Take an

example for ABC triblock copolymers, there are at least the following topological structures, as shown in Fig. 2.

Consider a system with volume V of n ABC triblock copolymers. The degree of polymerization of the block copolymer is N and the A, B, and C blocks consist of f_AN, f_BN, and f_CN monomers, respectively. Each polymer is parameterized with the variable s, which increases along each chain.

In contrast to AB diblock copolymers, however, as the number of distinct blocks is increased from two to three, say ABC triblocks, both the complexity and variety of self-assembled structures are significantly increased. For example, the controlling parameters, such as χ_{AB}, χ_{AC}, χ_{BC}, f_A, f_B, f_C, N, and so on, could increase 18 times. In recent years, about 20 microphase structures have been found including core-shell lamellae, gyroids, cylinders and spheres, and their combinations, such as spheres in cylinders, cylinders in lamellae, rings on cylinders, and even some amazing knitting pattern[24,25]. Unfortunately, some of these new structures are found theoretically and not yet confirmed by the experimental work.

Using a real space implementation of the self-consistent field theory (SCFT) for polymeric system proposed by Drolet and Fredrickson[17], we develop an efficient SCFT algorithm for complex architectures of multiblock copolymers[22]. By using this method, we explore microphases of ABC linear triblock copolymers in a two dimensional space. Seven microphases are found to be stable for the ABC triblock in 2D, which include lamellae, hexagonal lattice, core-shell hexagonal lattice, tetragonal lattice, lamellae with beads inside, lamellae with beads at the interface, and hexagonal phase with beads at the interface, as shown in Fig. 3.

By systematically varying the composition, triangle phase diagrams are constructed for four classes of typical triblocks in terms of the relative strengths of the interaction energies between different species (see ref. [22] for details). In general, when both the volume fractions and interaction energies of the three species are comparable, lamellar phases are found to be the most stable. While if one of the volume fractions is large, core-shell hexagonal, or tetragonal phase can be formed, depending on which of the blocks dominates. Furthermore, more complex morphologies, such as lamellae with beads inside, lamellae with beads at the interface, and hexagonal phase with beads at the interface compete for stability with lamellae structures, as the interaction energies between distinct blocks become asymmetric.

In particular, for ABC triblock copolymers, the phase behavior depends strongly on sequencing of the blocks. For example, when the volume fractions of three components are comparable, lamellae phase can be changed into core-shell structure. It is interesting to note that in the strong-segregation limit the same effect has also been examined by Zheng and Wang[16]. Experimentally, a lamellar phase in 1∶1∶1 poly (isoprene-*b*-styrene-*b*-2-vinylpyridine) (ISP) has been observed by Mogi *et al.*[26], while a co-axial cylinder phase was found in SIP by Gido *et al.*[27], as shown in Fig. 4. Our calculation based upon SCFT provides guidance to the design of new microstructures in complex block copolymers.

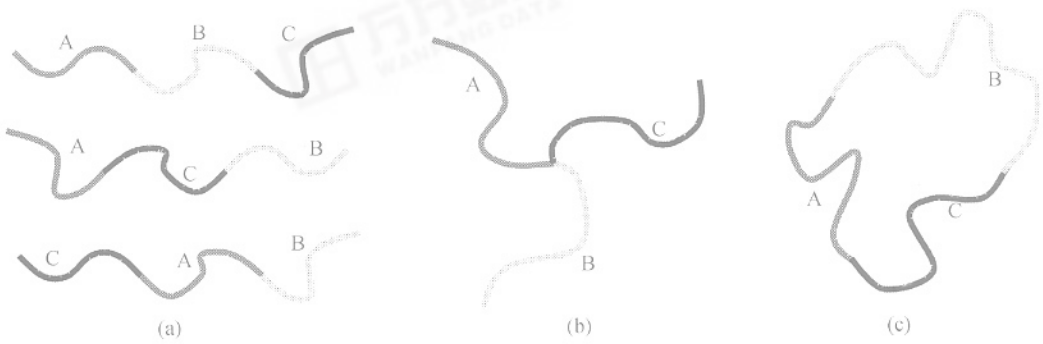

Fig. 2. Architectures of ABC triblock copolymers. (a) Linear, including different sequences of blocks, such as ABC, BCA, and CAB; (b) star; (c) ring.

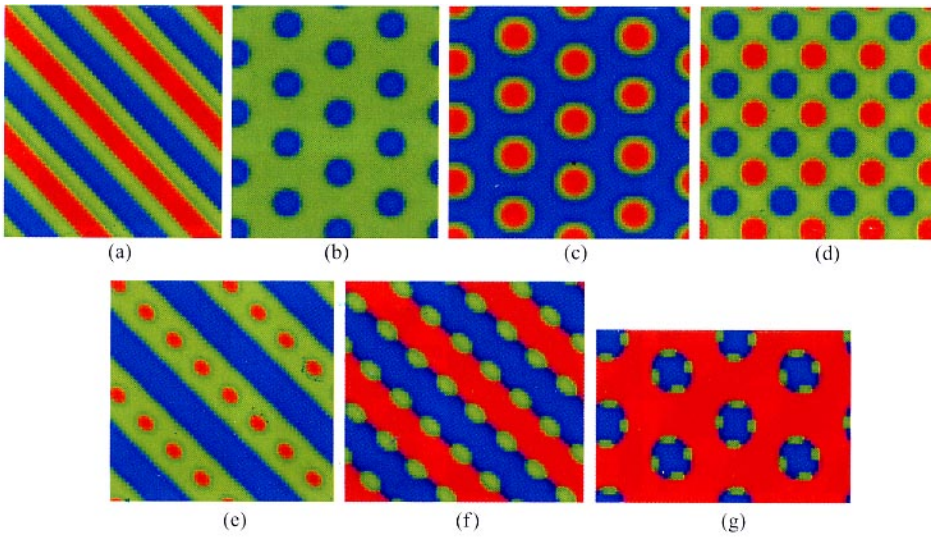

Fig. 3. Schematic ordered morphologies for ABC linear block copolymers. A (red), B (green) and C (blue). (a) "three color" lamellar phase (LAM_3); (b) hexagonal lattice phase (HEX); (c) core-shell hexagonal lattice phase (CSH); (d) two interpenetrating tetragonal lattice phase (TET_2); (e) lamellar phase with beads inside (LAM+BD-I); (f) lamellar phase with beads at the interface (LAM+BD-II); (g) hexagonal phase with beads at the interface (HEX+BD)[22].

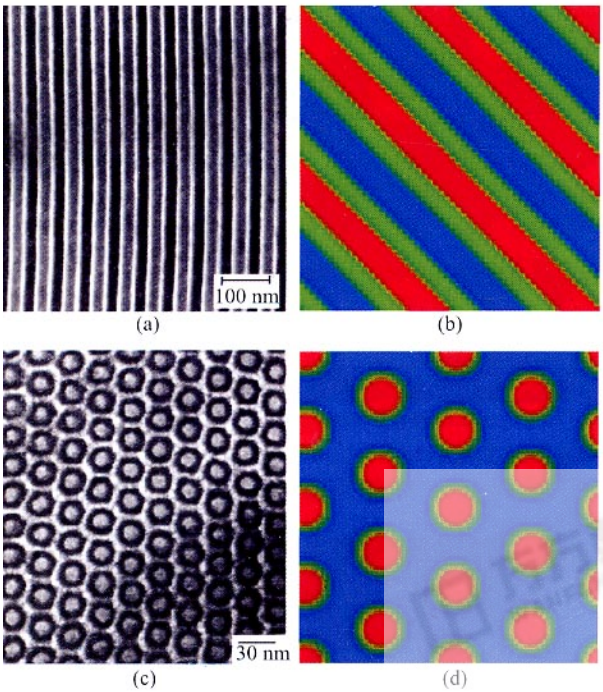

Fig. 4. (a) TEM morphologies of PS-PI-P2VP from ref. [26]; (c) TEM morphologies of linear BAC triblock copolymer PI-PS-P2VP from ref. [27]; (b) and (d) are corresponding calculated self-assembled morphologies of linear ABC and BAC copolymers by using SCFT[22].

In contrast to linear ABC triblocks, the microphase separation behavior of star ABC triblocks in Fig. 2(b) is more complicated due to the junction constraint of the center cores that regulates the geometry of the microphases formed[23]. In 2D, nine stable microphases are uncovered, shown in Fig. 5, including hexagonal lattice, core-shell hexagonal lattice, lamellae, lamellae with beads at the interface, as well as a variety of complex morphologies that are absent in linear ABC triblocks, such as "three-color" hexagonal honeycomb phase, knitting pattern, octagon-hexagon-tetragon phase, lamellar phase with alternating beads, and decagon-hexagon-tetragon phase. A similar morphology with the same composition is obtained by Gemma *et al*. in their Monte-Carlo simulations[28], by Liang *et al*. in terms of dynamic density functional[29], and Bohbot-Raviv and Wang in terms of density functional theory[30].

It is interesting to note that the recent experimental work by Takano and coworkers[31] confirms our simulation[23], as shown in Fig. 6. Three-color hexagonal honeycomb phase (HEX_3), 8-8-4, 10-6-4 and 12-6-4 phase characterized by TEM was found for PS-PI-P2VP star triblock copolymers, similar to our prediction. Moreover, our predicted phase is qualitatively in agreement with the experimental findings by Thomas *et al*.[32], who studied star triblocks of polystyrene (PS), polyisoprene (PI), and poly(methyl methacrylate) (PMMA).

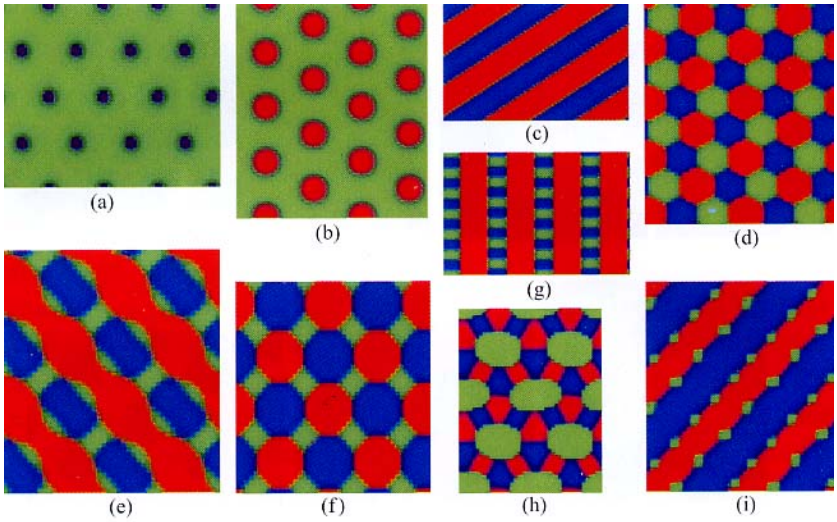

Fig. 5. Schematics of the 2D ordered microphases for ABC star triblock copolymers. A (red), B (green) and C (blue). (a) Hexagonal lattice phase (HEX); (b) core-shell hexagonal lattice phase (CSH); (c) "three-color" lamellar phase (LAM_3); (d) "three-color" hexagonal honeycomb phase (HEX_3); (e) knitting pattern (KP); (f) octagon-hexagon-tetragon phase (OHT); (g) lamellae phase with alternating beads (LAM+BD); (h) decagon-hexagon-tetragon phase (DEHT); (i) lamellae phase with beads at the interface (LAM+BD-I)[23].

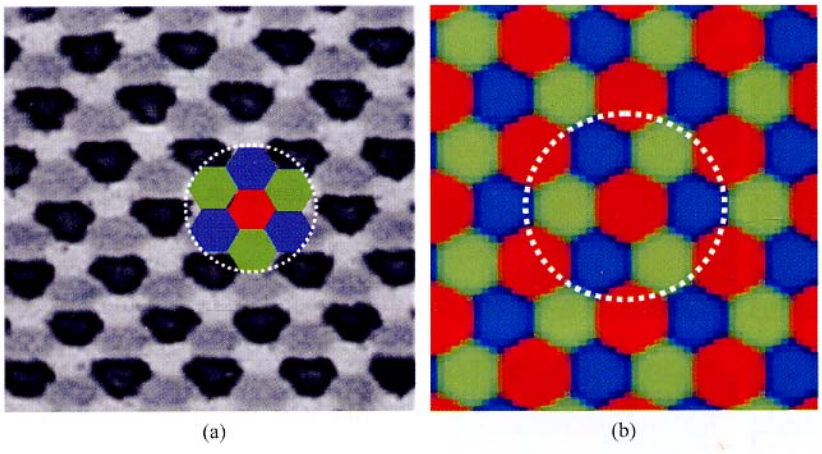

Fig. 6. (a) TEM morphologies (HEX_3) of star PS-PI-PMMA from ref. [31]; (b) our simulation morphology by using SCFT[23].

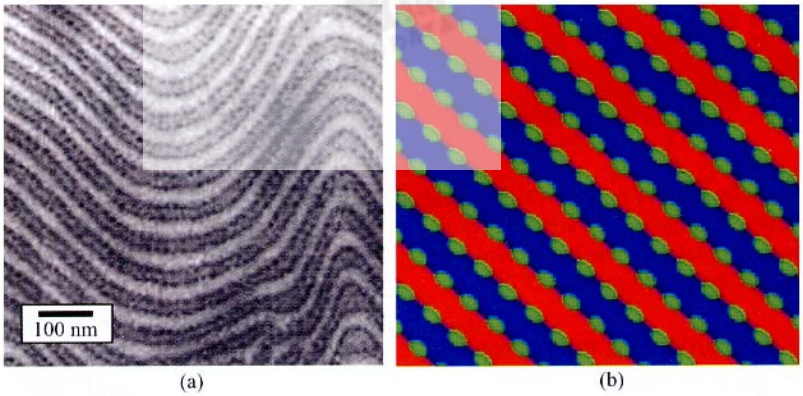

Fig. 7. (a) TEM morphologies (LAM+BD-II) of linear PS-PI-PMMA from ref. [31]; (b) our simulation morphology by using SCFT[23].

Furthermore, as shown in Fig. 7, the lamellae phase with beads at the interface (LAM+BD-I) found in Fig. 5(i) was also obtained by Takano and coworkers[31].

By systematically varying the composition, the triangle phase diagrams are constructed for ABC star triblocks both with symmetric and asymmetric interaction parameters among the three species[23]. It is found that when the volume fractions of the three blocks are comparable, the star architecture plays a profound role in the complex microphase formation. However, when one of the blocks is relatively short with χN values not very large, the star architecture is less important and therefore the phase behavior is similar to that of linear triblocks. In general, the triangle phase diagrams we present, as a first step, may be used as guidance to designing possible ordered structures of star ABC triblock copolymers in terms of the composition, and the values of interaction energies and their relative strengths.

3.2 Interfacial effects of flexible polymers with small molecular liquid crystals

Polymer composites containing liquid crystal have been developed for applications in the field of liquid crystal reinforced composites and especially display device. Concerning the forming process of liquid crystal, many physical properties of the liquid crystals are largely influenced by the interfacial effects[33−35]. The following will discuss the SCFT applications in polymeric systems with liquid crystals.

Owing to anisotropy of liquid crystals, the phase behavior of mixtures of flexible polymers and small liquid crystalline molecules is quite complicated. By combining Flory-Huggins solution theory and Maier-Sauper or Lebwohl-Lasher liquid crystal theory, the free energy and static phase diagram of mixtures of flexible polymers and small molecular liquid crystals have been obtained by our group[36,37]. The results showed that the coexistence of liquid-liquid and liquid-nematic two-phase regions is due to the ordering of the liquid crystal, which are consistent with those obtained by Monte Carlo simulation[38]. We also studied the interface of mixtures by using Lebwohl-Lasherliquid crystal and Helfand lattice SCFT[39], and verified the results with Monte Carlo simulation[40]. However, theoretical results reveal that flexible polymers are almost excluded completely from the ordered liquid crystal rich phase to form narrow interface due to the ordering of liquid crystal molecules when liquid-nematic phase separation occurs. As a result, the interface size is comparable to the lattice size leading to the lattice model only suitable for the case of shallow quench, namely wide interface. Thereby it is desired to develop continuum SCFT instead of lattice SCFT for a wide range of applications.

For the anisotropic liquid crystal system, Maier-Saupe interaction Hamilton (eq. (20)) must be included and is introduced to general SCFT in sec. 2 to obtain the following SCFT equations[41]:

$$\begin{aligned} W_{\mathrm{p}}(\mathbf{r}) &= \chi_{\mathrm{pl}}\phi_{\mathrm{l}}(\mathbf{r}) + \xi(\mathbf{r}) + \lambda_{\mathrm{p}}, \\ W_{\mathrm{l}}(\mathbf{r}) &= \chi_{\mathrm{pl}}\phi_{\mathrm{p}}(\mathbf{r}) + \xi(\mathbf{r}) + \lambda_{\mathrm{l}}, \end{aligned} \tag{25}$$

$$\begin{aligned} \phi_{\mathrm{p}}(\mathbf{r}) &= \frac{\bar{\phi}_{\mathrm{p}}V}{N_{\mathrm{p}}Q_{\mathrm{l}}}\int_0^{N_{\mathrm{p}}} \mathrm{d}s q(\mathbf{r},s)q(\mathbf{r},N_{\mathrm{p}}-s), \\ \phi_{\mathrm{l}}(\mathbf{r}) &= \frac{\bar{\phi}_{\mathrm{l}}V}{Q_{\mathrm{p}}}\int \mathrm{d}(\cos\theta)\ \mathrm{e}^{-\psi(\mathbf{r},\cos\theta)P_2(\cos\theta)}, \end{aligned} \tag{26}$$

$$\begin{aligned} \psi(\mathbf{r},\cos\theta) &= -\chi_{\mathrm{ll}}\int \mathrm{d}(\cos\theta')S(\mathbf{r},\cos\theta'), \\ S(\mathbf{r},\cos\theta) &= \frac{\bar{\phi}_{\mathrm{l}}V}{Q_{\mathrm{l}}}\mathrm{e}^{-\psi(\mathbf{r},\cos\theta)P_2^2(\cos\theta)}, \end{aligned} \tag{27}$$

$$Q_{\mathrm{l}}[\omega_{\mathrm{l}},\psi] = \int \mathrm{d}\mathbf{r}\mathrm{e}^{-\omega_{\mathrm{l}}(\mathbf{r})}\int \mathrm{d}(\cos\theta)\ \mathrm{e}^{-\psi(\mathbf{r},\cos\theta)P_2(\cos\theta)},$$

$$\begin{aligned} Q_{\mathrm{p}}[\omega_{\mathrm{l}},\psi] &= \int D\mathbf{R}_{\mathrm{p}}(s)\mathrm{e}^{-\frac{3}{2b^2}\int_0^{N_{\mathrm{p}}}\mathrm{d}s\left(\frac{\partial\mathbf{R}_{\mathrm{p}}(s)}{\partial s}\right)^2}\mathrm{e}^{-\int_0^{N_{\mathrm{p}}}\mathrm{d}s\omega_{\mathrm{p}}[\mathbf{R}_{\mathrm{p}}(s)]} \\ &= \int \mathrm{d}\mathbf{r}q(\mathbf{r},N_{\mathrm{p}}), \end{aligned} \tag{28}$$

$$\phi_{\mathrm{p}}(\mathbf{r}) + \phi_{\mathrm{l}}(\mathbf{r}) = 1, \tag{29}$$

where $P_2(\cos\theta)$ is second Legendre function, λ_{p} and λ_{l} are Lagrange multipliers to ensure constant concentration ϕ_{p} and ϕ_{l}, respectively. χ_{pl} and χ_{ll} are Flory-Huggins isotropic interaction between polymers and liquid crystals and Maier-Saupe anisotropic interaction between liquid crystal molecules, respectively. The segment distribution function of flexible polymers $q(\mathbf{r}, s)$ satisfies the following diffusion equation with initial condition $q(\mathbf{r}, 0) = 1$:

$$\frac{\partial q(\mathbf{r},s)}{\partial s} = \left[\frac{b^2}{6}\nabla^2 - \omega_{\mathrm{p}}(\mathbf{r})\right]q(\mathbf{r},s). \tag{30}$$

When spatial inhomogeneousness is neglected, the equations in refs. [36, 37] for liquid crystal polymeric

systems can be recovered from the above equation (30). Moreover, by taking advantage of the thermodynamics, the equilibrium phase diagram is readily obtained[36,42]. As we only care the interfacial property in the following discussion, the above SCFT equations can be solved only along the interface normal, say z.

The calculated interfacial density and orientation order parameter profiles are shown in Fig. 8. It is shown by Fig. 8(a) that the interface between flexible polymers and liquid crystals is very narrow, only ~1.2b. When liquid crystal rich phase goes into polymer rich phase, the decrease of liquid crystal concentration at the interface undergoes similar first order phase transition of liquid crystal orientation order parameter, shown in Fig. 8(b).

Obviously, when the repulsive interaction between polymers and liquid crystals or anisotropic interaction between liquid crystal molecules is strong, the interface will be narrower and the liquid crystal concentration in polymer rich phase is low. However, the concentration of polymers in liquid crystal rich phase is relatively low and is not affected by the value of χ_{pl} since the situation of polymers in liquid crystals is not favorable for the conformation entropy. The orientation parameter S of liquid crystal rich phase depends on the value of χ_{ll}, the bigger χ_{ll}; the larger S.

It is not surprising that the width of the interface and interfacial tension depend on the polymer length. In Fig. 9, when the phase separation is driven by the ordering of liquid crystals, the increase of the length of flexible polymers leads to increase in repulsive interaction between polymers and liquid crystals, while the width of the interface ς is constant with variation of polymer length.

Furthermore, the basic results by using continuum SCFT developed by our group are consistent with those obtained by Helfand lattice interface model[39] and lattice Monte Carlo simulations[40]. We believe that continuum SCFT covers a wide range of applications and should be very useful for designing liquid crystal polymeric materials.

3.3 Interactions between brush-coated clay sheets and polymer matrix

Polymeric nanocomposites are composed of polymers and dispersed inorganic particles with at least one dimension at nanoscale. It is now generally understood that for polymeric nanocomposites to achieve these improved properties the inorganic particles have to be molecularly dispersed within the polymer matrix[43]. In practice, however, the van der Vaals interactions between the inorganic particles are always attractive, which result in the aggregation or flocculation of the particles. It is, thus, important to tailor the surfaces of the particles to control the surface force. One common means is to end-graft polymer chains onto the particle surfaces, forming what is usually referred to as a *polymer brush.* Although the scaling analyses were rather successful in giving qualitative prediction and interpretation of experimental observations[44−47], they were limited in providing detailed information about the specific density profiles and interactions of the polymer brush/melt systems. Using a continuous one dimensional self-consistent field theory, Ferreira *et al.* performed a systematic exploration of the parameter space of a polymer protected surface in contact with a

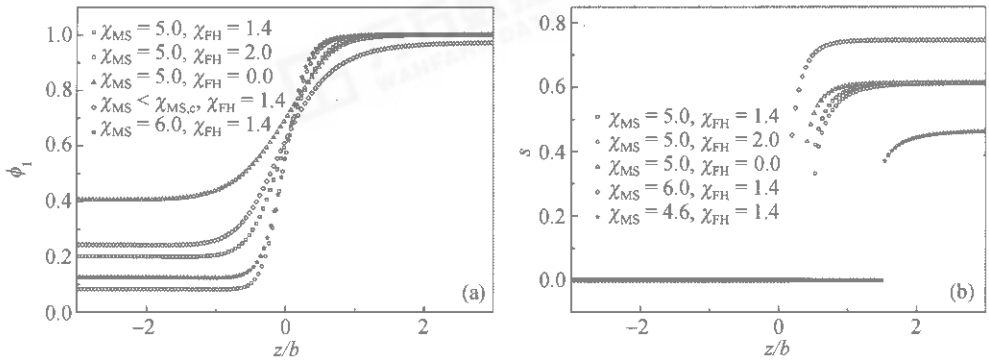

Fig. 8. (a) Variation of interfacial density profiles $\phi_1(z)$ with different interaction parameters ($\propto 1/kT$); (b) orientation order parameter along the interface. The distance from the interface is measured in unit of Kuhn length[41].

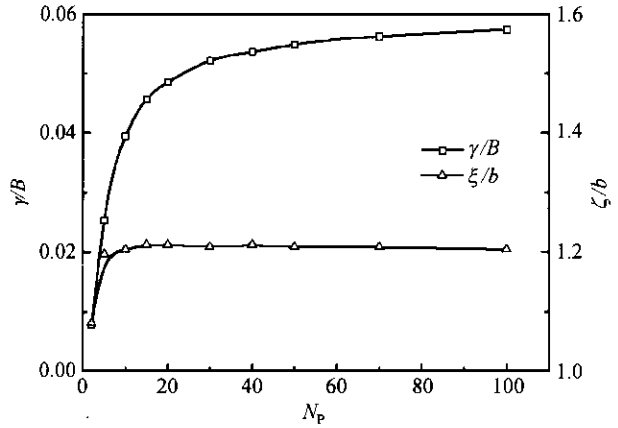

Fig. 9. Dependence of the interfacial width and the interfacial tension upon the chain length of polymers with $\chi_{II} = 5.0$, $\chi_{Ip} = 0$[41].

melt[48]. Their calculation shows that due to subtle entropic effects the melt chains are expelled from the grafted layer, even if they are chemically identical to the grafted chains, and the interactions between the clay sheets can be purely repulsive or repulsive at short distances and attractive at longer distances. However, such scaling regimes with intermediate sheet length, which is important to applications of nano-sheets, have entirely been left out by the previous theoretical studies. Attempting to deal with this practically useful case of intermediate sheet lengths, here we report numerical calculations that do not impose any assumption on the sheet length. By using the continuum SCF formulism originally developed by Edwards and extended to multicomponent mixtures by Hong and Noolandi, the morphologies and interaction potentials of the brushcoated clay sheets/polymer melt system have been carried out by our group[49].

We consider a system of two parallel clay sheets with a distance H along the x-axis and grafted with n_α polymer chains of polymerization index N (Fig. 10) and the grafting density of the grafted chains is given by

$$\sigma = bn_\alpha / 4(L+W), \tag{31}$$

where L and W are the lateral length along the z-axis and the thickness of the clay sheets, respectively. The average volume fraction of the grafted chains is defined as

$$\bar{\psi}_\alpha = \frac{n_\alpha N}{\rho_0 V}, \qquad \bar{\psi}_\beta = \frac{n_\beta N_\beta}{\rho_0 V}, \tag{32}$$

where n_β and N_β are the number and the length of polymer chains, respectively; V is the volume and ρ_0 is the reference density.

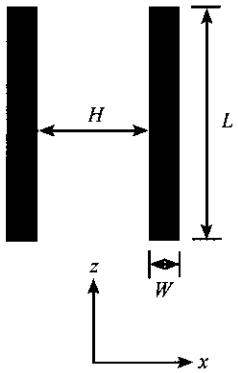

Fig. 10. Schematic diagram illustrating the variables used in the calculation. Note that H is the distance between the two front surfaces of the clay sheets[49].

The probability, $q_\alpha(\mathbf{r}, s)$, that a grafted chain ends at $\mathbf{r}$ in s steps having started at the surfaces of the clay sheets satisfies a modified diffusion equation (eq. (30)), but with the initial condition, $q_\alpha(\mathbf{r} = \mathbf{r}_c, 0) = 1$, $q_\alpha(\mathbf{r} \neq \mathbf{r}_c, 0) = 0$, and the boundary condition $q_\alpha(\mathbf{r} = \mathbf{r}_c, s) = 0$. Because the two ends of the grafted chains are distinct, a second end-segment distribution function, $q^*_\alpha(\mathbf{r}, N_\alpha) = 1$, is needed according to eq. (17), with the initial condition, $q^*_\alpha(\mathbf{r}, N_\alpha) = 1$, and the boundary condition, $q^*_\alpha(\mathbf{r} = \mathbf{r}_c, s) = 0$. For the free chains β, the two ends are identical, therefore, only one end-segment distribution function is needed, and the equation of $q_\beta(\mathbf{r}, s)$ is similar to eq. (30) with the initial condition, $q_\beta(\mathbf{r}, 0) = 1$, and the boundary condition, $q_\beta(\mathbf{r}=\mathbf{r}_c, s) = 0$. These SCFT equations can be real space implemented.

The interaction between the two polymer brushes also alters the structure of the brushes. As an example, we first illustrate in Fig. 11 the distribution of the monomer density for two clay sheets at different distances H. In Fig. 12, we present the free energy plots as a function of the distance H for different values of grafting densities and lateral lengths, respectively. From Fig. 12, we can clearly see that the minimum of the free energy appears at higher grafting density and

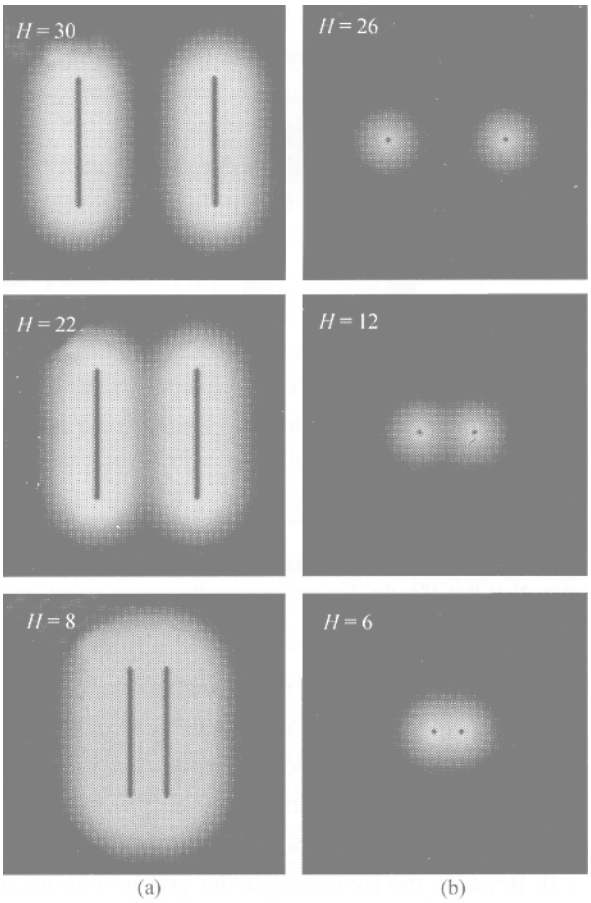

Fig. 11. Distribution of total monomer density of the grafted chains. (a) $N_\alpha = N_\beta = 50$, $\sigma = 0.25$, $L = 31$, $W = 3$; (b) $N_\alpha = N_\beta = 50$, $\sigma = 0.25$, $L = 3$, $W = 3$. The monomer density in the white region is higher than that in the dark region and the dark rectangles with different lengths in the center of the white region represent the clay sheets[49].

longer lateral length, when the distance between the two front surfaces is relative, for example, H~22. Furthermore, higher grafting density and longer lateral length are favorable for large brush separations, and hence for repulsive interaction. In other words, the clay sheets may arrange periodically. These findings may have various implications for creating novel polymeric nanocomposites.

As shown in Fig. 13, we calculate in a systematic way the locus of points N, P, L, and σ at which the attractive interaction disappears. For the fixed value of N, P, and L, the grafting density was varied until the first value of σ, for which the free energy of interaction becomes negative, was found. Obviously, the result can be the guidance to the design of polymeric nanocomposites.

As shown in Fig. 10, the mass center of the two sheets has the same z coordinates. For more common cases, the coordinates of mass center of the two sheets are set to be $(x, z) = (H_{//}, H_\perp)$, $H_{//}$ is the distance of the mass center along x direction, and $H_\perp$ is the distance of the mass center along z direction. The free energy as a function of $(H_{//}, H_\perp)$ is shown in Fig. 14[50].

We should mention that it is straightforward to extend the present 2D model to other complicated systems. For example, when the lateral length L and the thickness W of the sheet are comparable, this model can be used for spherical clay. In summary, the results in terms of continuum SCFT indicate that the structureand interactions of the brush-coated clay sheets can be tailored by varying the grafted chain length and/or the lateral length of the clay sheets to benefit the fabrication of polymer/clay nanocompo-

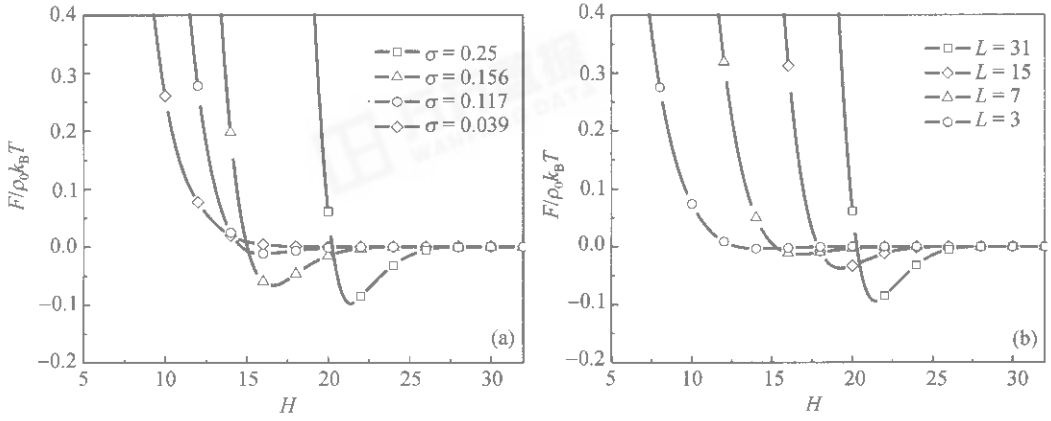

Fig. 12. (a) Free energy of interaction of two brushes as a function of the distance H for different grafting densities, $N_\alpha = N_\beta = 50$, $L = 31$, $W = 3$; (b) free energy of interaction of two brushes as a function of the distance H for different lateral lengths, $N_\alpha = N_\beta = 50$, $\sigma = 0.25$, $W = 3$[49].

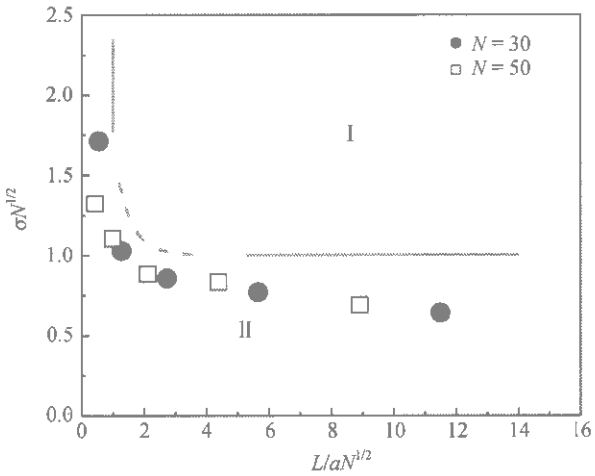

Fig. 13. Locus of points (N, σ, L) that characterize the beginning of the expulsive of the mobile chains from the grafted layer. Results are presented for N= P = 30 (filled circles) and N = P = 50 (squares). The solid and dashed curves are the sketch of the proposed scaling function. Region I denotes an interaction with an attractive part and region II denotes a purely repulsive interaction.

sites.

3.4 Shape transformation of fluid vesicles anchored by polymers

Biological membrane is not only the basic unit of the cell structure, but also the structural foundation to provide the life activity. Biological membrane is in close relation with many life processes, such as energy transformation, substance transportation, signal recognition and transduction, cell growth and differentiation, and nerve conduction. The backbone of the cell membrane is given by the self assembled lipid bilayer. In biological systems, the membranes are often "decorated" by a large number of macromolecules, such as proteins, cholesterol and carbohydrate. for example, membrane-spanning proteins embedded in the plasma membrane of animal cell. The glycocalyx is formed by coupling the polysaccharose brush with the membrane-spanning proteins on the cell outside[51]. As shown in Fig. 15, the vesicle which is anchored by polymer chains is a simplified model of biological cell. The vesicle membrane usually is impenetrable by most biomacromolecules. Complex shape changes, such as budding, pearling, and coiling of the vesicles, can be induced even when a very small amount of polymer chains are anchored and/or adsorbed onto the membranes[52,53]. These subtle shape changes of vesicles with anchored polymers have also drawn theoretical attention[54−56]. Analytical calculations and Monte Carlo simulations reveal that the anchored chains can induce local inhomogeneities of the bending rigidity and spontaneous curvature of the membrane[54,55]. Adsorption of polymers anchored to membranes was also investigated and for strong adsorption a decrease of the entropically induced membrane curvature was predicted[57]. So far, theoretical studies have accounted for the altering of the spontaneous curvature and bending rigidity of an infinitively large planar membrane. For vesicles, however, due to the closure of the membranes, a different model for closed vesicles with anchored polymers, which has more biological relevance, is needed. We proposed an approach that combines the Helfrich curvature elasticity theory for fluid

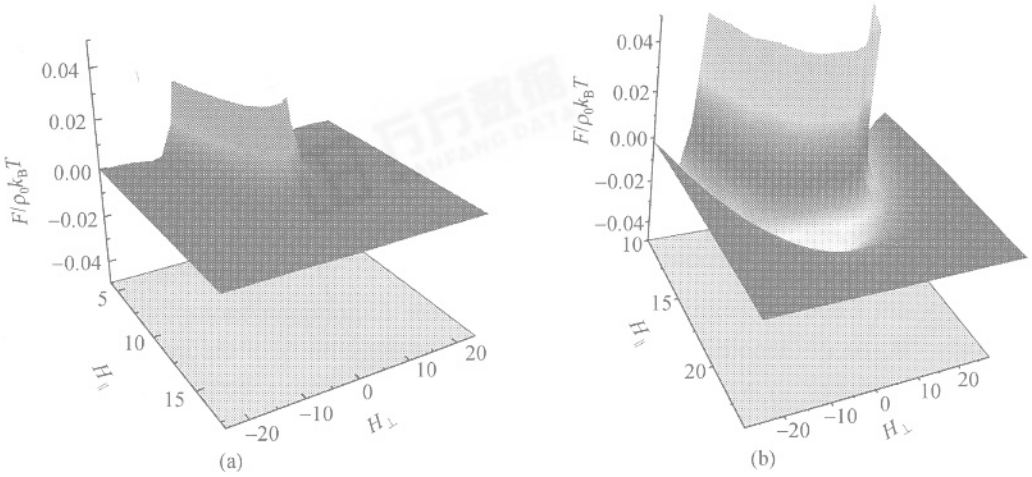

Fig. 14. The free energy of interactions as a function of ($H_{//}$, $H_\perp$) for different grafting densities, N_α= N_β= 50, L = 31, W = 3. (a) σ = 0.039, no attractive interactions well; (b) σ = 0.25, appearance of attractive interactions well[50].

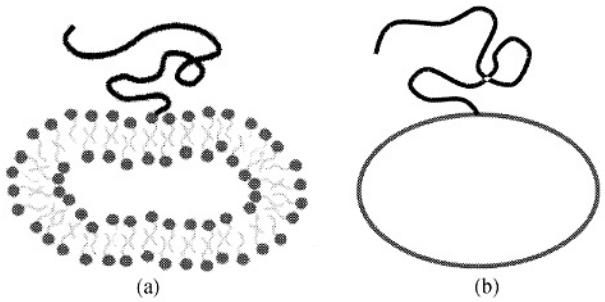

Fig. 15. (a) Vesicle anchored by polymer chain; (b) a simplified schematic model of (a).

membranes and the self-consistent field theory (SCFT) for polymers to satisfy this need. The Helfrich theory has been extensively used to explore the shape changes of closed membranes under various conditions. The diskocyte shape of the red blood cell has been successfully predicted[58]. For polymer systems, SCFT is the method of choice for numerical studies of equilibrium phases. The combined Helfrich-SCFT theory allows the simultaneous prediction of the shapes of vesicles with anchored polymer chains as well as the segment distributions of these chains[59].

Consider a polymer-vesicle system in Fig. 15(b). We assume that the vesicle membrane is infinitively thin but not penetrable by the polymer chains that are outside the vesicle. The number of solvent molecules is n_s and that of the polymer chains is n_p with each chain of n_p segments. The partition function of such a system can be written as

$$\Xi = \frac{1}{n_s!n_p}\int\prod_{i=1}^{n_s} D\mathbf{R}_s^i \int\prod_{i=1}^{n_p} D\mathbf{R}_p^i(\tau)\mathrm{e}^{-\beta H_p^0[\mathbf{R}_p^i(\tau)]} \times\int D\mathbf{R}_m(u,v)\mathrm{e}^{-\beta H_m^0}\mathrm{e}^{-\beta H_{int}} \times\prod_{\mathbf{r}}\delta[\hat{\rho}_p(\mathbf{r})+\hat{\rho}_s(\mathbf{r})-\rho_0]\delta\left[\int_{\mathbf{r}\in V_{in}[\mathbf{R}_m(u,v)]}\mathrm{d}\mathbf{r}\hat{\rho}_p(\mathbf{r})\right], \quad (33)$$

where $\beta = k_BT$, and $\int D\mathbf{R}$ denotes functional integration over configurations of the solvents, polymers, and fluid membrane. $\mathbf{R}_s^i$ and $\mathbf{R}_p^i(\tau)$ denote the spatial positions of the solvent i and the segment τ of the i chain, respectively. $\mathbf{R}_m(u,v)$ denotes the spatial position of the membrane and (u, v) are curvilinear coordinates in the membrane surface. $\mathbf{r}\in V_{in}[\mathbf{R}_m(u,v)]$ or $\mathbf{r}\in V_{out}[\mathbf{R}_m(u,v)]$ denotes that $\mathbf{r}$ is inside or outside the volume enclosed by the vesicle membrane, respectively. The first δ-function ensures the incompressibility constraint and ρ_0 is the reference density, and the second δ-function guarantees that the membrane is impenetrable by polymer chains. The density operators are defined as $\hat{\rho}_s(\mathbf{r}) = \sum_{i=1}^{n_s}\delta(\mathbf{r}-\mathbf{R}_s^i)$, and $\hat{\rho}_p(\mathbf{r}) = \sum_{i=1}^{n_p}\int_0^{N_p}\mathrm{d}\tau\chi[\mathbf{r}-\mathbf{R}_p^i(\tau)]$, and the interaction Hamiltonian includes interactions between the polymer segments and solvent molecules and the membrane, i.e., $H_{int} = V_{ps} + V_{pm}$, which can be written as $\beta V_{ps} = \chi\int\mathrm{d}\mathbf{r}\hat{\rho}_s(\mathbf{r})\hat{\rho}_p(\mathbf{r})$ and $\beta V_{pm} = \eta\int\mathrm{d}u\mathrm{d}v\hat{\rho}_p\{\mathbf{r}\in A[\mathbf{R}_m(u,v)]\}$, where χ and η are the interaction parameters of polymer-solvent and polymer-membrane pairs, respectively, and $A[\mathbf{R}_m(u,v)]$ represents the surface of the closed vesicle membrane. The Hamiltonian of the polymer chain can be written as $\beta H_p^0[R_p] = (3/2b^2)\int_0^{N_p}\mathrm{d}\tau[\partial R_p(\tau)/\partial\tau]^2$, where b is the Kuhn length of the chain. The Hamiltonian of the vesicle can be written as[60]

$$\beta H_m^0 = (\kappa/2)\int_{\mathbf{R}_m(u,v)}\mathrm{d}u\mathrm{d}v(2H+c_0)^2 + \lambda\int_{\mathbf{R}_m(u,v)}\mathrm{d}u\mathrm{d}v + \Delta p\int_{\mathbf{r}\in V_{in}[\mathbf{R}_m(u,v)]}\mathrm{d}\mathbf{r}, \quad (34)$$

where H and c_0 are the local mean curvature and spontaneous curvature of the fluid membrane, respectively. κ is the bending rigidity of the membrane, λ can be considered as the tensile stress acting on the membrane, and $\Delta p = p_{out} - p_{in}$ is the pressure difference across the membrane. Following the standard procedure of the SCFT as described above, the following the self-consistent equations can be obtained[6]:

$$\omega_p = \begin{cases}\eta/b+\chi\rho_s+\xi, & \mathbf{r}\in A[\mathbf{R}_m],\\ \zeta+\chi\rho_s+\xi, & \mathbf{r}\in V_{in}[\mathbf{R}_m],\\ \chi\rho_s+\xi, & \mathbf{r}\in V_{out}[\mathbf{R}_m],\end{cases} \quad (35)$$

$$\omega_s = \chi\rho_p+\xi, \quad (36)$$

where Lagrangian multipliers ξ as well as ς denote incompressibility of the system and impenetrability of the membrane, respectively.

$$\rho_p = \frac{n_p}{Q_p}\int_0^{N_p}\mathrm{d}\tau q_p(\mathbf{r},\tau)q_p^*(\mathbf{r},\tau), \quad (37)$$

where the definition of q_p and Q_p is the same as eqs.

(13) and (14).

$$\rho_{\mathrm{s}}=\frac{n_{\mathrm{s}}}{Q_{\mathrm{p}}}\mathrm{e}^{-\omega_{\mathrm{s}}},\quad \rho_{\mathrm{s}}+\rho_{\mathrm{p}}=\rho_0,\quad \int_{\mathbf{r}\in V_{\mathrm{in}}[\mathbf{R}_{\mathrm{m}}]}\mathrm{d}\mathbf{r}\rho_{\mathrm{p}}. \quad (38)$$

Following the standard procedure of the functional minimization for fluid membranes[60], we obtain the shape equation of the vesicle in the presence of polymers:

$$\begin{aligned}&\{\Delta p+\zeta\rho_{\mathrm{p}}(\mathbf{r}=\mathbf{R}_{\mathrm{m}})+\eta\mathbf{n}\cdot\nabla\rho_{\mathrm{p}}(\mathbf{r}=\mathbf{R}_{\mathrm{m}})\}\\&-2\{\lambda+\eta\rho_{\mathrm{p}}(\mathbf{r}=\mathbf{R}_{\mathrm{m}})\}H+2\kappa\nabla^2H\\&+\kappa(2H+c_0)(2H^2-c_0H-2K)=0,\end{aligned} \quad (39)$$

where **n** is the unit normal vector and K is the Gaussian curvature of the membrane.

In contrast to the general shape equation of vesicles derived by Ou-Yang and Helfrich[60], extra (inhomogeneous) pressure and tensile stress terms appear in eq. (39). The extra pressure $\zeta\rho_{\mathrm{p}}(\mathbf{r}=\mathbf{R}_{\mathrm{m}})$ originates from the reduction of the chain conformation entropy due to the spatial confinement of the polymer chains by the impenetrable membrane. The extra tensile stress $\eta\rho_{\mathrm{p}}(\mathbf{r}=\mathbf{R}_{\mathrm{m}})$ comes from the adhesion of the chain segments onto the vesicle membrane, which simply reflects that if the membrane adsorbs the chain, it reduces the tensile stress. Moreover, the adhesion of polymer chains onto the membrane also results in additional pressure $\eta\mathbf{n}\cdot\nabla\rho_{\mathrm{p}}(\mathbf{r}=\mathbf{R}_{\mathrm{m}})$, which also reflects that the membrane tends to contact more polymer segments if it adsorbs polymer segments.

To demonstrate our combined Helfrich-SCFT approach for exploring vesicle shapes under the effect of polymer chains, we have chosen to first investigate the system in which only a single polymer chain is anchored to the vesicle and restrict our study to a vesicle with axisymmetric shape. The dimensionless parameters were introduced in the numerical computation, $\tilde{\kappa}\to\kappa k_{\mathrm{B}}T$, $\tilde{\lambda}\to\lambda k_{\mathrm{B}}T/b^2$, $\Delta\tilde{p}\to\Delta p k_{\mathrm{B}}T/b^3$, $\tilde{\eta}\to\eta k_{\mathrm{B}}Tb$, $\tilde{\chi}\to\chi k_{\mathrm{B}}Tb^3$ and $\tilde{\zeta}\to\zeta k_{\mathrm{B}}T$. The length unit is $\sqrt{N_{\mathrm{p}}}b$ in the following figures of this section. The detailed numerical algorithm can be found in ref. [59].

In this article, we only show some typical results and the discussions of relevant physical property[59]. As shown in Fig. 16, the vesicle anchored by polymers exhibit various stable and metastable shapes.

In Fig. 16, we set η = 0.0 which means that the interaction between the vesicle and chain segment is not considered. But as shown in Fig. 17, the shape of vesi-

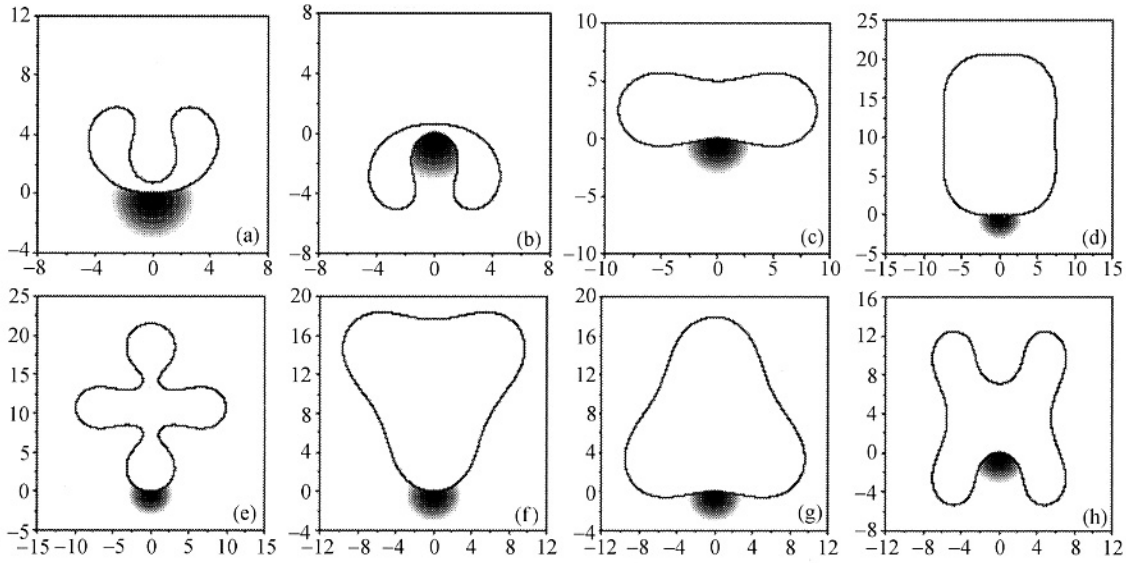

Fig. 16. Typical stationary solutions, including shapes of vesicle and segment distributions of the anchored polymer chain, to the self-consistent equations (35)−(39). The shape of the vesicle is represented by the solid curve and the density of the polymer chain is drawn in gray scale on a logarithmic scale. $\chi=\eta$ = 0.0.

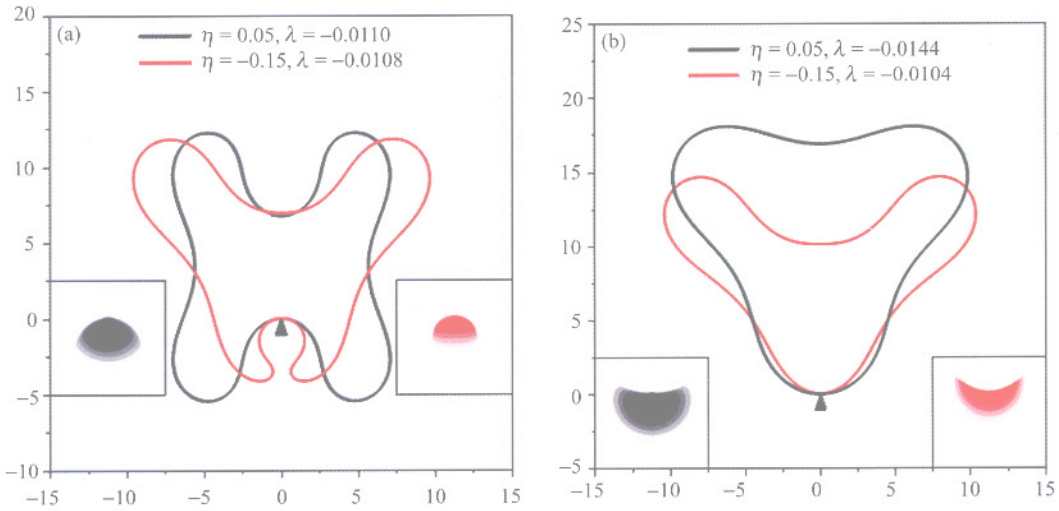

Fig. 17. Effect of polymer-membrane interaction parameter η on the vesicle shapes.

cles can be changed remarkably when there are interactions between the vesicle and chain segment.

As shown in Fig. 18, when the tubular vesicle is anchored by polymers, vesicle will exhibit pearling instability. Tsafrir *et al*.[52] have observed the pearling of vesicle when very few polymer chains were adsorbed onto the surface of vesicle. The similar result is obtained when vesicle is anchored by one polymer chain. Instead of tubular vesicle, the pearling vesicle became a stable solution. This can be used to explain the pearling instability when slight disturbance was exerted on the tubular vesicle. Moreover, wherever vesicle is anchored by the polymer, the pearling vesicle is always a stable solution of shape equation.

In general, polymer can be anchored to inside of vesicle. We show an example of polymer anchored to outside and inside of vesicle in Fig. 19[61].

This method can readily be extended to the system of infinite membrane anchored by flexible polymer and completely stiff polymer (rod). In ref. [62], we discussed the local shape of the infinite membrane anchored by rod and compared relevant results with the infinite membrane anchored flexible polymer.

3.5 Self-assembled morphologies of block copolymers in solution

Another application of SCFT is in the field of self-assembled morphologies simulation of block copolymers in solution. Amphiphilic block copolymers can self-assemble to form various complex microstructures, such as rod-, sphere-like micelles and vesicles, depending on the preparation conditions, such as the composition and the temperature. The aggregate formation is of fundamental and practical interests as they have many potential applications in areas such as microreactors, microcapsules and drug delivery system[63]. Liang and coworkers[64,65] first investigate the aggregate morphologies of AB diblock copolymers in dilute solution by using SCFT in 2D. The aggregate morphologies dependence self-assembled from amphiphilic ABC triblock copolymers in solution, on the interaction parameters between different blocks, have been investigated by the real-space implementation of SCFT by our group[66]. As mentioned above, SCFT equations (17), (21)—(24) for bulk block copolymers can be conveniently extended to block copolymer solution[66]. In contrast to diblock copolymers in solution, the aggregation of triblock copolymers is more complicated due to the presence of the second hydrophobic blocks and hence big ranges of parameter space controlling the morphology. For simplicity, the end block A is assumed as hydrophilic ($\chi_{AS}N$ = 0.5) and short enough and the other two blocks B and C are hydrophobic and relatively long to ensure the so-called crew-cut copolymers. The composition of block copolymers is taken to be f_A = 0.1, f_B = 0.15 and f_C = 0.75 with the end block C being the major component in all simulations. Thus, we focus on considering the effect of the hydrophobicity of two blocks B and C of

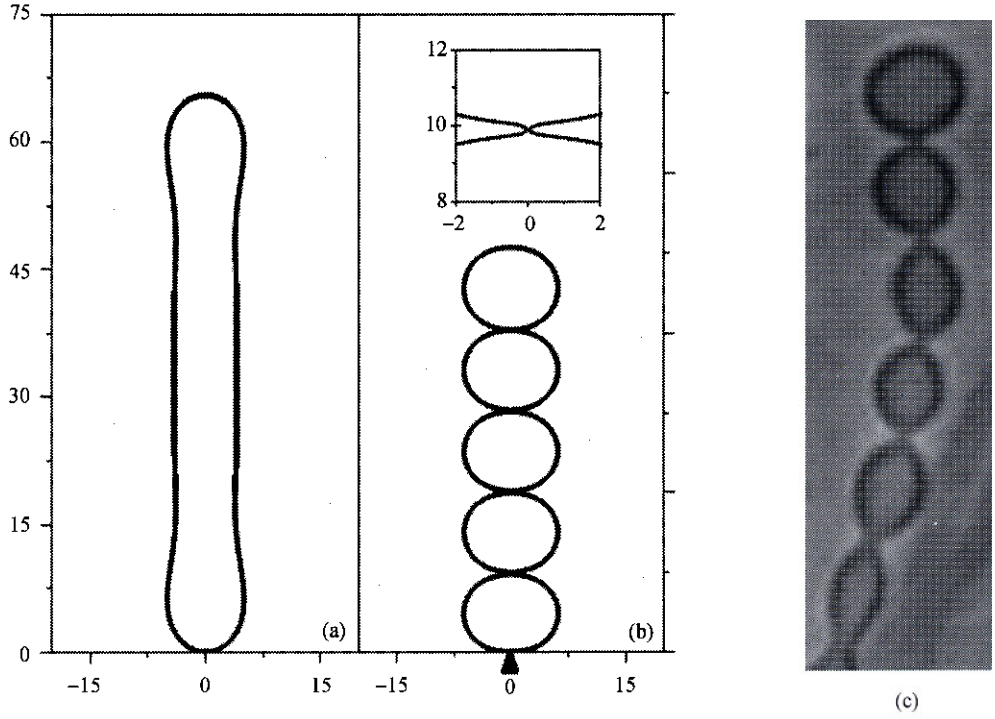

Fig. 18. (a) The tubular vesicle is obtained with parameters $\kappa = 1.67$, $\chi = \eta = 0.0$, $\Delta p = 0.00001$, $c_0 = 0$, $\lambda = -1.5(\Delta p/2)^{2/3}$, $\varsigma = 1.5$; (b) the pearling vesicle is found with the same parameters, but a polymer chain with N_p=200 anchored[59]; (c) the pearling vesicle was observed in the experiment[52].

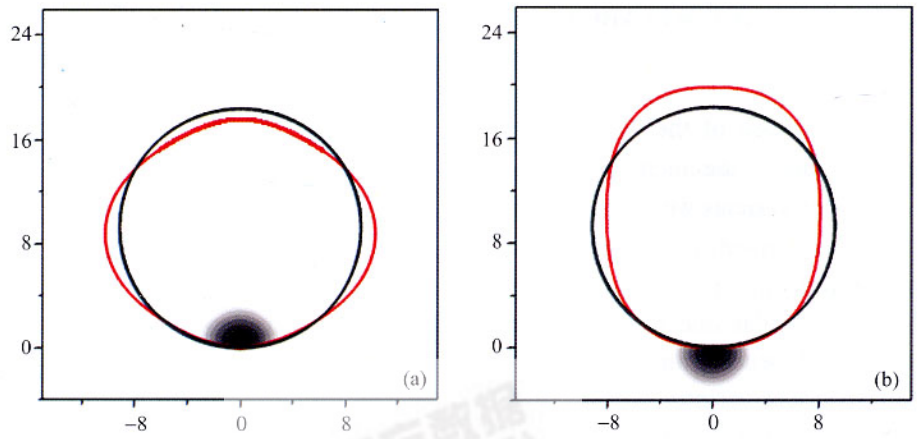

Fig. 19. (a) Shapes of polymer anchored vesicle inside ($\tilde{\zeta} = -300$); (b) shapes of polymer anchored vesicle outside ($\tilde{\zeta} = 300$); $\tilde{\chi} = 0.0$, $c_0 = 0.0$, $\tilde{\chi} = 0.0$, $\tilde{\eta} = 0.0$, $\Delta\tilde{p} = 0.03$, $\tilde{\lambda} = -0.1375$, $\tilde{\kappa} = 1.67$. The shape of the vesicle is represented by solid curve (the red solid line is the vesicle anchored by polymer with $N_p = 200$, the black solid line is the vesicle without polymer anchoring).

linear ABC block copolymer on the aggregate morphology. The concentration of block copolymers is set as $f_p = 0.1$. We further assume the interaction parameters of the three different blocks are equal, i.e., $\chi_{AB}N = \chi_{AC}N = \chi_{BC}N = \chi N$. Similar to the implementation of SCFT equations for block copolymers in bulk, as mentioned above, we solved the SCFT in 2D for amphilic ABC triblock copolymers in dilute solution[66].

Similar to the self-assembly of block copolymers in bulk, the segregation degree of different blocks has significant influence on the morphology of block copolymers in solution as well. As shown in Fig. 20, at

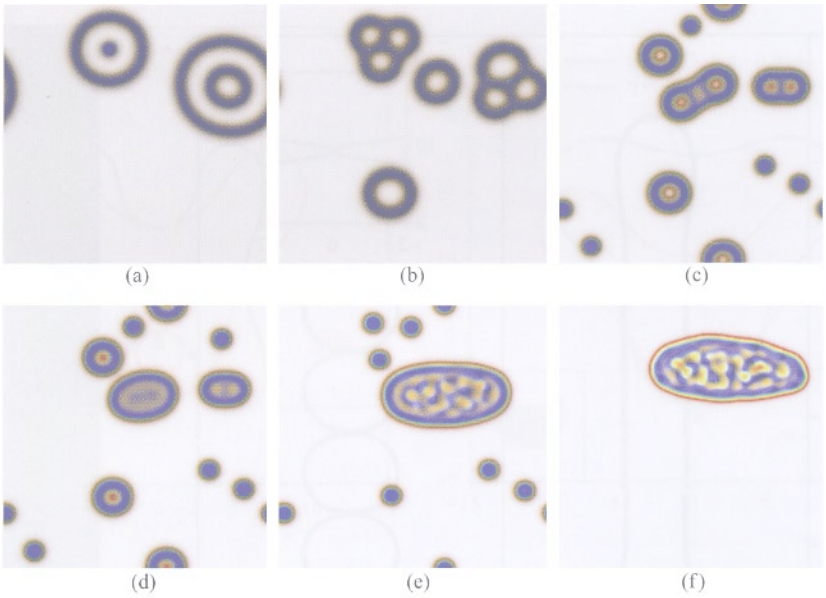

Fig. 20. Morphology of amphiphilic ABC triblock copolymer in dilute solution with χN =15 (weak segregation) and $\chi_{AS}N$ = 0.5 [66]. A (red), B (green) and C (blue). (a) $\chi_{BS}N = \chi_{CS}N$ = 21.5; (b) $\chi_{BS}N = \chi_{CS}N$ = 22; (c) $\chi_{BS}N = \chi_{CS}N$ = 25; (d) $\chi_{BS}N = \chi_{CS}N$ = 26; (e) $\chi_{BS}N = \chi_{CS}N$ = 30; (f) $\chi_{BS}N = \chi_{CS}N$ = 40.

the condition of χN = 15, namely the copolymer is in the weak-segregation regime, there exists the competition between polymers macrophase separation from the solvent and microphase separation in ABC triblock copolymers, which is absent in AB diblock copolymer systems[66].

In Fig. 20, with the increase of the degree of the hydrophobic property, namely the increase of $\chi_{BS}N$ ($=\chi_{CS}N$), various shapes of vesicles were found in Fig. 20 (a)—(c). The vesicles formed a three-phase five-layer ABCBA lamellar structure in contrast to the two-phase three-layer ABA lamellar one for diblock copolymers. We noted that Eisenberg and coworkers[63] reported the similar spherical vesicles prepared from PS_{180}-$PMMA_{67}$-$PtBuA_{37}$ linear triblock copolymer solution. But with further increasing $\chi_{BS}N$ ($=\chi_{CS}N$), which means that the solubility for blocks B and C decreases, the solvent cannot mix with the blocks B and C, and the interfacial tension goes up, then the block copolymer tends to macro-separate from the solvent and thus forms large size of the micellar aggregates. Once the interactions between the solvent and the hydrophobic blocks B and C become very strongly repulsive, the repulsive forces between the A, B and C blocks cannot balance the repulsion from the solvent, therefore, the hydrophobic block C prefers to self-assembly into the inner part of the phase to completely avoid the contact with the solvents, then the system will macro-separate. It should be pointed out that the phenomena due to the competition between macrophase and microphase separation existing in linear ABC triblock copolymer system, however, are absent for diblocks. Furthermore, when the block copolymer is in strong segregation regime, there is no coexistence of macrophase and microphase separation at all, as shown in Fig. 20[66].

From Fig. 21, in contrast to the case of weak segregation, the interface between different blocks becomes clear due to the relatively strong interactions among the different blocks. It is important to note that compared to the case of weak segregation in Fig. 20, the macrophase separation does not exist, while peanutlike and long linelike micelles occur instead. However, the weak hydrophobic condition favors the vesicle formation similar to the case of weak segregation. The vesicle-to-circlelike micelle transition is found with increasing the hydrophobicities of the blocks B and C.

The block sequence of linear ABC triblock copolymers has large influence on the phase behavior, and thus, we check the effects of different hydrophobicity of blocks B and C on the morphologies when the middle block B is strongly hydrophobic. For example, $\chi_{BS}N$ = 30, the morphologies are shown in Fig.

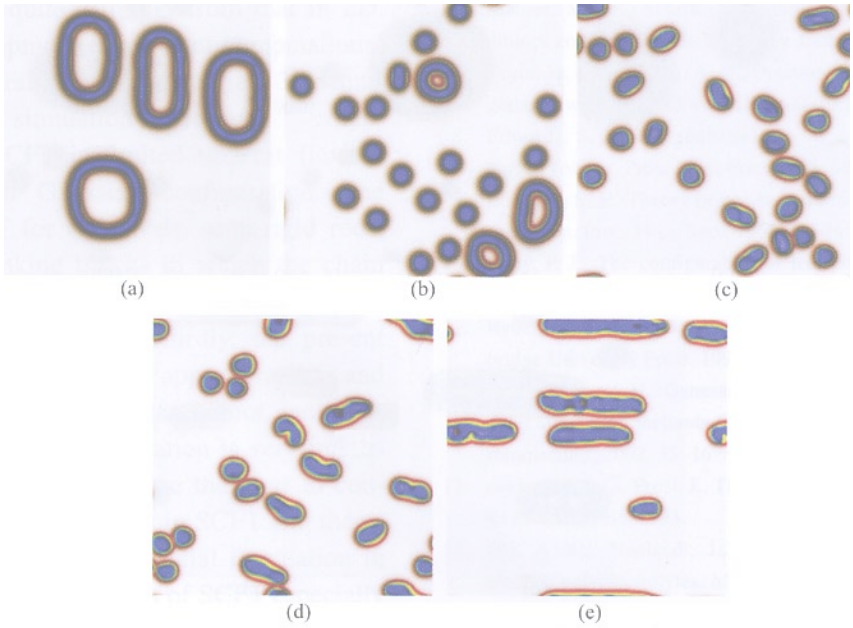

Fig. 21. Morphology of amphiphilic ABC triblock copolymer in dilute solution with $\chi N = 35$ (strong segregation) and $\chi_{AS}N = 0.5$ [66]; A (red), B (green) and C (blue). (a) $\chi_{BS}N = \chi_{CS}N = 26$; (b) $\chi_{BS}N = \chi_{CS}N = 28$; (c) $\chi_{BS}N = \chi_{CS}N = 35$; (d) $\chi_{BS}N = \chi_{CS}N = 40$; (e) $\chi_{BS}N = \chi_{CS}N = 50$.

22 for $\chi N = 15$, $\chi_{AS}N = 0.5$. When $\chi_{CS}N < \chi_{BS}N$, i.e., the middle block B is most hydrophobic, the weaker hydrophobic block C, which is the major component of the copolymer, tends to partially mix with hydrophilic block A. As a response, the microphase separation exists at the interface between the solvent and the block copolymer resulting in obscure interface between the block copolymer and the solvent. In this case, large compound micelles are observed and the block copolymers are in a disordered state due to the weak segregation degree of the block copolymer. With increasing of the hydrophobicity of the block C, the boundaries both among the different blocks and between the copolymer and the solvent become distinguished and develop a core-shell-shell structure of the block copolymer, then the coexisting of large compound micelles with the general small micelles occurs, as shown in Fig. 22(b) and (c). But when $\chi_{CS}N$ further increases to lager than $\chi_{BS}N$, i.e., $\chi_{CS}N > \chi_{BS}N$, the long linelike micelles are found, as shown in Fig. 22(d) and (e)[66].

3.6 Other applications of SCFT

Despite the above mentioned examples, the SCFT applications are very versatile and the following briefly lists further advances of SCFT in polymeric system.

(1) One of the important application areas of SCFT is dealing with microphase separation of block copolymers under confinement condition. Actually, in many cases, the microphase separation is not in the free space, but is in a physically confined environment, such as block copolymers confined in a film[67] or in a nanochannel[68]. The mesostructures produced by confined syntheses are useful as templates for fabricating highly ordered mesostructured nanowires and nanowire arrays, and thus studies of confinement effects of block copolymers have attracted much attention theoretically[68,69]. For the simple case of copolymers confined in a thin film, strong-segregation theory can be used to deal with microphase morphologies[69]. However, for more complex confinement condition, SCFT is the best method to investigate the phase behavior just by adjusting the boundary condition of diffusion equation (17) and interactions between the polymer and confinement boundary[68,70].

(2) It is well known that A/B binary blends phase separate following two mechanisms, namely nucleation-growth (NG) and spinodal. SCFT has been employed successfully to investigate the NG phase sepa

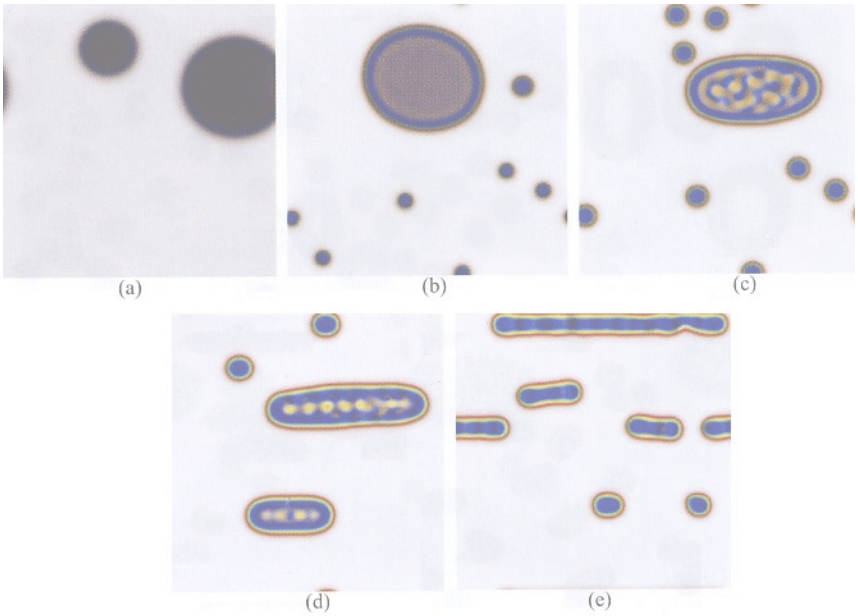

Fig. 22. Morphology of amphiphilic ABC triblock copolymer in dilute solution with $\chi N = 15$ (weak segregation), $\chi_{AS}N = 0.5$ and $\chi_{BS}N = 30$ [66]. A (red), B (green) and C (blue). (a) $\chi_{CS}N = 20$; (b) $\chi_{CS}N = 25$; (c) $\chi_{CS}N = 30$; (d) $\chi_{CS}N = 35$; (e) $\chi_{CS}N = 40$.

ration of A/B binary blends[71]. We employed SCFT to study more complex nucleation mechanism. For example, effects of AB diblock copolymers to A/B binary blends on the structure and nucleation were investigated by using SCFT[72]. We also studied the nucleation of A/B binary blends in the presence of mesoscopic spherical particles[73]. We further investigated the nucleation nature of disordered micelles in highly asymmetric, sphere-forming diblock copolymer melts by employing SCFT[74]. These studies are of great importance to understand phase sepration mechanism and clear some uncertainties of experimental results in this area[71−74].

(3) In the above applications of SCFT, although thermodynamic equilibrium properties are considered, it should be emphasized that the SCFT technique is very flexible and versatile. In particular, incorporation of dissipative dynamics, SCFT may serve as dynamic SCFT, namely DSCFT (dynamic self-consistent field theory) [75]. We employed DSCFT to investigate microphase separation dynamics for linear ABC triblock copolymers (see ref. [75] for details).

(4) Thompson and coworkers[76] proposed a theoretical model based SCFT and density functional theory to treat nanocomposites composed of block copolymers and inorganic nanoparticles. Furthermore, SCFT have been extended to deal with the phase behavior of polyeletrolyte system[77] and block copolymers with nanoparticles[78].

4 Summary and outlook

In summary, in the past two decades, the SCFT is based on the Gaussian model, which includes three contributions, namely interaction energy between different species, entropy from stretching of the chain and impressibility of the system. Many ideas of modern condensed matter and field-based theory are introduced into the SCFT and thus inspiring developments have been made. Concerning the applications, the phase behavior for flexible polymers predicted by SCFT is quantitatively in agreement with the experimental observations. In particular, the SCFT shows great ability to treat the microphase separation morphologies at equilibrium state. Despite the great success of SCFT, owing to the complexity of polymeric systems, at least the following listings are still a challenging task. Firstly, most of work in this area is carried out in 2D due to the great computational challenge. Although most of the 2D structure can provide enough and important information of 3D morphology, the 3D structure of complicated morphologies such as Gyroid for complex multiblock copolymers with com-

plex architectures is quite different from that in 2D. Therefore, the development of efficient computational technique, such as parallel algorithm to treat 3D simulation and large-size simulation is desired[79,80]. Secondly, the present SCFT is limited to treat flexible polymer chains with Gaussian configuration. The formulation of SCFT for rigid rods, semi-rigid rods, crystalline or crosslinking blocks in which the chain cannot be properly described by Gaussian configuration is still a great challenge. Thirdly, the present SCFT is based on the mean-field approximation, and thus, the concentration fluctuation is not included. However, the concentration fluctuation is very important for dilute polymer system. One then has to consider the spatial correlation effects in SCFT and therefore, how to introduce the time-spatial fluctuation in the SCFT is the key to applications of SCFT especially in dilute block copolymer solution. Fourthly, extension of SCFT to deal with the mechanics properties of inhomogeneous polymer complex fluid, such as the viscoelasticity, is highly desired in respect of polymer materials. To our knowledge, DSCFT might be a promising starting point to tackle this problem. Finally, the remaining challenging problem for the future in this field is applying SCFT in various biological macromolecules related to the life system. We speculate that the SCFT could be very useful and efficient dealing with the folding of proteins and biological cell evolution, which are of high interest in biology.

Acknowledgements This work was supported by the National Basic Research Program of China (Grant No. 2005CB623800) and the National Natural Science Foundation of China (Grant Nos. 20474012, 20374016 & 20104002).

References

1. Hadjichristidis, N., Pispas, S., Floudas, G., Block Copolymers, Hoboken: John Wiley & Sons, 2003.
2. Leibler, L., Theory of microphase separation in block copolymers, Macromolecules, 1980, 13: 1602－1617.
3. Semenov, A. N., Contribution to the theory of microphase layering in block-copolymer melts, Sov. Phys. JEPT, 1985, 61: 733－742.
4. Milner, S. T., Witten, T. A., Cates, M. E., A parabolic density profile for grafted polymers, Europhys. Lett., 1988, 5: 413－418.
5. Matsen, M. W., The standard Gaussian model for block copolymer melts, J. Phys: Condens. Matter, 2002, 14: R21－R47.
6. Matsen, M. W., Schick, M., Stable and unstable phases of a diblock copolymer melt, Phys. Rev. Lett., 1994, 72: 2660－2663.
7. Feynman, R. P., Hibbs, A. R., Quantum Mechanics and Path Integrals, New York: McGraw-Hill Book Company, 1965.
8. Edwards, S. F., The statistical mechanics of polymers with excluded volume, Proc. Phys. Soc., 1965, 85: 613－624.
9. Edwards, S. F., Theory of polymer solutions at intermediate concentration, Proc. Phys. Soc., 1966, 88: 265－280.
10. Flory, P. J., The configuration of real polymer chains, J. Chem. Phys., 1949, 17: 303－310.
11. Ryder, L. H., Quantum Field Theory, 2nd ed., Cambridge: Cambridge University Press, 1996.
12. Fredrickson, G. H., Ganesan, V., Drolet, F., Field-theoretic computer simulation methods for polymers and complex fluids, Macromolecules, 2002, 35: 16－39.
13. deGennes, P. G., Prost, J., The Physics of Liquid Crystals, Oxford: Clarendon press, 1993.
14. Shi, A. C., Noolandi, J., Theory of inhomogeneous weakly charged polyelectrolytes, Macromol. Theory Simul., 1999, 8: 214－229.
15. Helfand, E., Theory of inhomogeneous polymers: Fundamentals of the Gaussian random-walk model, J. Chem. Phys., 1975, 62: 999－1005.
16. Morse, D. C., Fredrickson, G. H., Semiflexible polymers near Interfaces, Phys. Rev. Lett., 1994, 73: 3235－3238.
17. Drolet, F., Fredrickson, G. H., Combinatorial screening of complex block copolymer assembly with self-consistent field theory, Phys. Rev. Lett., 1999, 83: 4317－4320.
18. Holden, G., Legge, N. R., Quirk, R. *et al*., Thermoplastic Elastomers, 2nd ed., Cincinnati: Hanser/Gardner Publishers, 1996.
19. Park, M., Harrison, C., Chaikin, P. M. *et al*., Block copolymer lithography: Periodic arrays of similar to 10(11) holes in 1 square centimeter, Science, 1997, 276: 1401－1404.
20. Archibald, D. D., Mann, S., Template mineralization of self-assembled anisotropic lipid microstructures, Nature, 1993, 364: 430－433.
21. Morkved, T. L., Wiltzius, P., Jaeger, H. M. *et al*., Mesoscopic self-assembly of gold islands and diblock-copolymer films, Appl. Phys. Lett., 1994, 64: 422－424.
22. Tang, P., Qiu, F., Zhang, H. D. *et al*., Morphology and phase diagram of complex block copolymers: ABC linear triblock copolymers, Phys. Rev. E, 2004, 69: 031803.
23. Tang, P., Qiu, F., Zhang, H. D. *et al*., Morphology and phase diagram of complex block copolymers: ABC star triblock copolymers, J. Phys. Chem. B, 2004, 108: 8434－8438.
24. Hamley, I. W., The Physics of Block Copolymers, Oxford: Oxford University Press, 1998.
25. Bates, F. S., Fredrickson, G. H., Block copolymers—Designer soft materials, Physics Today, 1999, 52: 32－38.
26. Mogi, Y., Kotsuji, H., Kaneko, Y. *et al*., Tricontinuous morphology of triblock copolymers of the ABC type, Macromolecules, 1992, 25: 5412－5415.

27. Gido, S. P., Schwark, D. W., Thomas, E. L. *et al*., Observation of a non-constant mean curvature interface in an ABC triblock copolymer, Macromolecules, 1993, 26: 2636—2640.
28. Gemma, T., Hatano, A., Dotera, T., Monte Carlo simulations of the morphology of ABC star polymers using the diagonal bond method, Macromolecules, 2002, 35: 3225—3237.
29. He, X. H., Huang, L., Liang, H. J. *et al*., Self-assembly of star block copolymers by dynamic density functional theory, J. Chem. Phys., 2002, 116: 10508—10513.
30. Bohbot-Raviv, Y., Wang, Z. G., Discovering new ordered phases of block copolymers, Phys. Rev. Lett., 2000, 85: 3428—3431.
31. Takano, A., Wada, S., Sato, S. *et al*., Observation of cylinder-based microphase-separated structures from ABC star-shaped terpolymers investigated by electron computerized tomography, Macromolecules, 2004, 37: 9941—9946.
32. Sioula, S., Hadjichristidis, N., Thomas, E. L., Direct evidence for confinement of junctions to lines in an 3 miktoarm star terpolymer microdomain structure, Macromolecules, 1998, 31: 8429—8432.
33. Doane, J. W., Vaz, N. A., Wu, B. G. *et al*., Field controlled light scattering from nematic microdroplets, Appl. Phys. Lett., 1986, 48: 269—271.
34. Ding, J. D., Yang, Y. L., Birefringence patterns of nematic droplets, Jpn. J. Appl. Phys., 1992, 31: 2837—2845.
35. Drzaic, P. S., Polymer dispersed nematic liquid crystal for large area displays and light valves, J. Appl. Phys., 1986, 60: 2142—2148.
36. Lin, Z. Q., Zhang, H. D., Yang, Y. L., Phase diagrams of mixtures of flexible polymers and nematic liquid crystals in a field, Phys. Rev. E, 1998, 58: 5867—5872.
37. Yang, Y. L., Lu, J. M., Zhang, H, D. *et al*., Phase-equilibria in mixtures of thermotropic small molecular liquid-crystals and flexible polymers, Polym. J., 1994, 26: 880—894.
38. Zhang, H. D., Li, F. M., Yang, Y. L., Statistical thermodynamics theory of phase equilibria in mixtures of thermotropic liquid-crystals and flexible polymers, Science in China, series B, 1995, 38: 412—421.
39. Chen, Y., Li, J., Zhang, H. D. *et al*., Theory of inhomogeneous polymers lattice model for the interface between flexible polymer and small molecular liquid crystal, Mol. Cryst. Liq. Cryst., 1995, 258: 37—50.
40. Zhu, J. X., Ding, J. D., Lu, J. M. *et al*., Monte Carlo simulation of the interface between flexible polymers and low molecular liquid crystals, Polymer, 39: 6455—6460.
41. Wang, J. F., Zhang, H. D., Qiu, F. *et al*., Self-consistent field theory of mixtures of flexible polymers and small liquid crystalline molecules, Acta Chimica Sinica (in Chinese), 2003, 62: 1180—1185.
42. Zhang, H. D., Lin, Z. Q., Yan, D. *et al*., Phase separation in mixtures of thermotropic liquid crystals and flexible polymers, Science in China, Series B, 1997, 40: 128—136.
43. Giannelis, E. P., Krishnamoorti, R. K., Manias, E., Polymer-silicate nanocomposites: Model systems for confined polymers and polymer brushes, Adv. Polym. Sci., 1999, 138: 107—147 and references therein.
44. de Gennes, P. G., Scaling Concepts in Polymer Physics, New York: Cornell University Press, 1985.
45. Aubouy, M., Fredrickson, G. H., Pincus, P. *et al*., End-tethered chains in polymeric matrices, Macromolecules, 1995, 28: 2979—2981.
46. Leibler, L., Ajdari, A., Mourran, A. *et al*., Ordering in Macromolecular Systems (eds. Teramoto, A., Kobayashi, M., Norisuji, T.), Berlin: Springer Verlag, 1994.
47. Gay, C., Wetting of a polymer brush by a chemically identical polymer melt, Macromolecules, 1997, 30: 5939—5943.
48. Ferreira, P. G., Ajdari, A., Leibler, L., Scaling law for entropic effects at interfaces between grafted layers and polymer melts, Macromolecules, 1998, 31: 3994—4003.
49. Wang, R., Qiu, F., Zhang, H. D. *et al*., Interactions between brush-coated clay sheets in a polymer matrix, Phys. Rev. E, 2003, 118: 9447—9456.
50. Wang, R., Self-assembly of polymer fluids based on self-consistent field theory, Postdoc Report in Fudan University (in Chinese), 2003.
51. Seifert, U., Lipowsky, R., Structure and Dynamics of Membranes (eds. Lipowsky, R., Sackmann, E.), Amsterdam: Elsevier Science B.V. 1995.
52. Tsafrir, I., Sagi, D., Arzi, T. *et al*., Pearling instabilities of membrane tubes with anchored polymers, Phys. Rev. Lett., 2001, 86: 1138—1141.
53. Frette, V., Tsafrir, I., Guedeau-Boudeville, M. A. *et al*., Coiling of cylindrical membrane stacks with anchored polymers, Phys. Rev. Lett., 1999, 83: 2465—2468.
54. Hiergeist, C., Lipowsky, R., Elastic properties of polymer-decorated membranes, J. Phys. II France, 1996, 6: 1465—1481.
55. Kim, Y. W., Sung, W., Membrane curvature induced by polymer adsorption, Phys. Rev. E, 2001, 63: 041910.
56. Breidenich, M., Netz, R. R., Lipowsky, R. *et al*., The shape of polymer-decorated membranes, Europhys. Lett., 2000, 49: 431—437.
57. Breidenich, M., Netz, R. R., Lipowsky, R. *et al*., Adsorption of polymers anchored to membranes, Eur. Phys. J. E, 2001, 5: 403—414.
58. Helfrich, W., Elastic properties of lipid bilayers—Theory and possible experiments, Z. Naturforsch, 1973, C 28: 693—703.
59. Wang, J. F., Guo, K. K., Qiu, F. *et al*., Predicting shapes of polymer-chain-anchored fluid vesicles, Phys. Rev. E, 2005, 71: 041908.
60. Ou-Yang, Z. C., Helfrich, W., Instability and deformation of a spherical vesicle by pressure, Phys. Rev. Lett., 1989, 59: 2486—2488.
61. Guo, K. K., Theoretical studies on the shapes of biological membranes, PhD Thesis in Fudan University (in Chinese), 2005.
62. Guo, K. K., Qiu, F., Zhang, H. D., Yang, Y. L., Predicting shapes of polymer-chain-anchored fluid vesicles, J. Chem. Phys., 2005, 71: 041908.

63. Yu, G., Eisenberg, A., Multiple morphologies formed from an amphiphilic ABC triblock copolymer in solution, Macromolecules, 1998, 31: 5546－5549.
64. He, X. H., Liang, H. J., Huang, L. *et al*., Complex microstructures of amphiphilic diblock copolymer in dilute solution, J. Phys. Chem. B, 2004, 108: 1731－1735.
65. Zhu, J. T., Jiang, Y., Liang, H. J. *et al*., Self-assembly of ABA amphiphilic triblock copolymers into vesicles in dilute solution, J. Phys. Chem. B, 2005, 109: 8619－8625.
66. Wang, R., Tang, P., Qiu, F. *et al*., Aggregate morphologies of amphiphilic ABC triblock copolymer in dilute solution using self-consistent field theory, J. Phys. Chem. B, 2005, 109: 17120－17127.
67. Lambooy, P., Russell, T. P., Kellogg, G. L. *et al*., Observed frustration in confined block copolymers, Phys. Rev. Lett., 1994, 72: 2899－2902.
68. Wu, Y. Y., Cheng, G. S., Katsov, K. *et al*., Composite mesostructures by nano-confinement, Nature Materials, 2004, 3: 816－822.
69. Yang, Y. Z., Qiu, F., Zhang, H. D. *et al*., Microphases of asymmetric diblock copolymers in confined thin films, Acta Chimica Sinica (in Chinese), 2004, 62: 1601－1606.
70. Yang, Y. Z., Block copolymers confined in thin films, Master Degree Thesis in Fudan University (in Chinese), 2006.
71. Wood, S. M., Wang, Z. G., Nucleation in binary polymer blends: A self-consistent field study, J. Chem. Phys., 2002, 116: 2289－2300.
72. Wang, J. F., Zhang, H. D., Qiu, F. *et al*., Nucleation in binary polymer blends: Effects of adding diblock copolymers, J. Chem. Phys., 2003, 118: 8997－9006.
73. Wang, J. F., Wang, Z. G., Yang, Y. L., Nucleation in binary polymer blends: Effects of foreign mesoscopic spherical particles, J. Chem. Phys., 2004, 121: 1105－1113.
74. Wang, J. F., Wang, Z. G., Yang, Y. L., Nature of disordered micelles in sphere-forming block copolymer melts, Macromolecules, 2005, 38: 1979－1988.
75. Xia, J. F., Sun, M. Z., Qiu, F. *et al*., Microphase ordering mechanisms in linear ABC triblock copolymers: A dynamic density functional study, Macromolecules, 2005, 38: 9324－9332.
76. Thompson, R. B., Ginzburg, V. V., Masten, M. W. *et al*., Predicting the mesophases of copolymer-nanoparticle composites, Science, 2001, 292: 2469－2472.
77. Wang, Q., Taniguchi, T., Fredrickson, G. H., Self-consistent field theory of polyelectrolyte systems, J. Phys. Chem. B, 2004, 108: 6773－6744.
78. Reister, E., Fredrickson, G. H., Nanoparticles in a diblock copolymer background: The potential of mean force, Macromolecules, 2004, 37: 4718－4730.
79. Sides, S. W., Fredrickson, G. H., Parallel algorithm for numerical self-consistent field theory simulations of block copolymer structure, Polymer, 2003, 44: 5859－5866.
80. Sun, M. Z., Microphase separation and shapes of vesicles based on self-consistent field theory, PhD Thesis in Fudan University (in Chinese), 2006.